REPORT DOCUMENTATION PAGE

Form Approved
OMB No. 0704-0188

1. REPORT DATE *(DD-MM-YYYY)*	2. REPORT TYPE	3. DATES COVERED *(From - To)*
31-03-2004	Final technical report	06-01-2002 to 12-31-2003

4. TITLE AND SUBTITLE

Space vector methods for AC drives to achieve high efficiency and superior waveform quality

5a. CONTRACT NUMBER
N00014-02-1-0751

5b. GRANT NUMBER
N00014-02-1-0751

5c. PROGRAM ELEMENT NUMBER

5d. PROJECT NUMBER

5e. TASK NUMBER

5f. WORK UNIT NUMBER

6. AUTHOR(S)

Raja Ayyanar, D. Zhao, H. Krishnamurthy, G. Narayanan
Arizona State University

7. PERFORMING ORGANIZATION NAME(S) AND ADDRESS(ES)

Arizona State University
Office for Research and Sponsored Projects Administration
PO Box 873503
Tempe, AZ 85287-3503

8. PERFORMING ORGANIZATION REPORT NUMBER

DWA0074/TE

9. SPONSORING / MONITORING AGENCY NAME(S) AND ADDRESS(ES)

Office of Naval Research
800 North Qunicy Street
Arlington, VA 22217-5660

10. SPONSOR/MONITOR'S ACRONYM(S)
ONR

11. SPONSOR/MONITOR'S REPORT NUMBER(S)

12. DISTRIBUTION / AVAILABILITY STATEMENT

Approved for public release; distribution is unlimited.

13. SUPPLEMENTARY NOTES
N/A

14. ABSTRACT

Space vector approach to pulse width modulation offers several advantages over the traditional triangle comparison methods, which are not fully exploited by conventional space vector PWM (SVPWM). New sequences, which divide the active vector duration, offer additional degrees of freedom that are not possible in triangle comparison approach. The objectives of this research are to identify all such new sequences and develop new PWM techniques that reduce distortion and switching loss.

Four new sequences involving active state division are introduced. The concept of stator flux ripple is used to design THD-optimized PWM techniques. By applying different sequences within a sector based on above techniques, THD can be reduced by 47% compared to conventional SVPWM. The effects of sequences on inverter switching loss are analyzed to design a new hybrid PWM that reduces switching loss by 30%. This involves using sequences that clamp the phase with the highest current, and double switch the phase with lowest current. Finally, a combined hybrid PWM technique that simultaneously reduces THD by over 30% and switching loss by 20%, under nominal conditions is developed. The new techniques have been implemented in a 2kW induction motor drive controlled by a DSP - TMS320F243. THD reduction of 38% in the THD-optimized PWM and switching loss reduction of 30% in the loss-optimized PWM are demonstrated. Future work in this area may focus on extending the concept to multi-level inverters.

15. SUBJECT TERMS
Pulse width modulation, motor drive, active state division, harmonic distortion, Switching loss, hybrid PWM

16. SECURITY CLASSIFICATION OF:			17. LIMITATION OF ABSTRACT	18. NUMBER OF PAGES	19a. NAME OF RESPONSIBLE PERSON
a. REPORT	b. ABSTRACT	c. THIS PAGE			Raja Ayyanar
UU	UU	UU	UU	71	19b. TELEPHONE NUMBER *(include area code)* (480) 727 7307

SPACE VECTOR METHODS FOR AC DRIVES TO ACHIEVE HIGH EFFICIENCY AND SUPERIOR WAVEFORM QUALITY

ONR Award No.: N00014-02-1-0751

Final Report

Submitted to:

Office of Naval Research

Program Officer: Terry S. Ericsen

ONR 334

Submitted by:

Arizona State University

PI: Raja Ayyanar

Phone: 480-727-7307

rayyanar@asu.edu

March 31, 2004

TABLE OF CONTENTS

EXECUTIVE SUMMARY 2

LIST OF FIGURES 3

1. INTRODUCTION 6

Motivation and objectives of the research project..... 6

Popular PWM techniques..... 6

2. NEW SEQUENCES INVOLVING DIVISION OF ACTIVE STATE DURATION 12

Derivation of all possible sequences..... 12
Distinguishing features of sequences involving active state division..... 17

3. THD CHARACTERISTICS OF NEW SEQUENCES..... 22

Analysis based on stator flux ripple..... 23

4. HYBRID PWM TECHNIQUES TO REDUCE THD..... 28

General procedure for the design of different PWM techniques..... 28
Experimental setup..... 30
Three-zone hybrid PWM technique I: *0127, 0121* and *7212*..... 30
Three-zone hybrid PWM technique II: *0127, 1012* and *2721*..... 35
Five-zone hybrid PWM technique..... 36
Seven-zone hybrid PWM technique..... 38

5. HYBRID PWM TECHNIQUES TO REDUCE SWITCHING LOSS..... 42

Possibility of reducing switching loss..... 42
Effect of different sequences on the switching losses..... 43
Switching loss optimized hybrid PWM technique..... 47
Experimental results..... 49

6. HYBRID PWM TECHNIQUES FOR SIMULTANEOUS REDUCTION IN THD AND SWITCHING LOSS..... 52

Hybrid PWM technique based on quality factor..... 53
Practical Hybrid PWM techniques for reduction of THD and switching loss.... 55
Hybrid PWM techniques with current feedback..... 59

7. CONCLUSIONS AND FUTURE WORK..... 66

Suggestions for future work..... 68

REFERENCES..... 69

APPENDIX A: LIST OF PUBLICATIONS FROM THIS WORK..... 71

EXECUTIVE SUMMARY

PWM techniques used in voltage source inverters for motor drives have a significant impact on the distortion in motor currents and switching losses in the inverter. The space vector approach to PWM offers several advantages over the traditional triangle comparison methods. However, the conventional space vector PWM (SVPWM) does not fully exploit these advantages, and is widely considered to be equivalent to triangle comparison approach. However, new sequences in SVPWM, which divide the active vector duration, offer additional degrees of freedom that are not possible in triangle comparison approach. The main objectives of this research are to identify all such new sequences, analyze their characteristics and develop new hybrid PWM techniques that reduce distortion and switching loss.

Four new sequences involving active state division have been introduced. The concept of stator flux ripple is applied systematically to analyze the effects of the new sequences on THD. Three hybrid PWM techniques that divide the space vector plane into zones of superior performance for different sequences have been developed. By applying different sequences within a sector based on the above zone division, the THD can be reduced by as much as 47% compared to conventional SVPWM, at maximum modulation index.

The effects of different sequences on the inverter switching loss also have been analyzed. A switching-loss-optimized PWM has been developed by dividing the α–ϕ plane into zones of superior performance for different sequences. This hybrid PWM can reduce the switching losses by more than 30% over a wide range of power factor angles. In general, to minimize the switching losses, the sequence that clamps the phase with the highest current, and double switches the phase whose current is near zero, should be chosen.

Finally, using the results obtained from the independent THD and switching loss studies, new hybrid PWM techniques that simultaneously reduce both THD and inverter switching losses have been developed, specifically for motor drive applications. These techniques achieve a reduction of over 30% in THD and a reduction of over 20% in switching loss simultaneously, while operating at nominal fundamental frequency of 60 Hz and at power factor angles close to 30^0 lagging.

The new PWM techniques have been implemented and validated on an experimental prototype comprising of a 2kW IGBT-based VSI fed induction motor drive controlled by a DSP - TMS320F243. THD reduction of 38% in the THD-optimized PWM and switching loss reduction of 30% in the switching-loss-optimized PWM have been demonstrated experimentally. With faster DSP clock frequency, experimental results will match even closer to the analytical results.

Future work in this area may focus on analyzing the effects of new sequences on the input current ripple, which affects the reliability of input capacitors, and on extending the concept of active state division to multi-level inverters.

LIST OF FIGURES

Figure Page

1. Three-phase voltage source inverter for motor drives. 7
2. Block diagram of a voltage source inverter fed AC motor drive....7
3. Different modulating waves used in triangle comparison approach....8
4. Switching states and voltage vectors of a voltage source converter. 9
5. Variation of THD with modulation index for different PWM techniques....10
6. Conventional and existing bus clamping sequences. 12
7. Derivation of possible sequences that result in two switchings in a sub-cycle. 14
8. Derivation of possible sequences that result in three switchings in a sub-cycle. ..14
9. All possible sequences satisfying the imposed constraints. 15
10. PWM waveforms corresponding to each of the seven sequences at a fundamental frequency of 50 Hz and an average switching frequency of 1 kHz. 16
11. Generation of PWM corresponding to *0127* using triangle comparison method ..18
12. Generation of PWM corresponding to *012* using triangle comparison method. ...19
13. Generation of PWM corresponding to *0121* using triangle comparison method. .20
14. Generation of PWM corresponding to *7212* using triangle comparison method. .20
15. Stator flux ripple corresponding to sequence *0127*....23
16. Stator flux ripple corresponding to bus clamping sequences *012* and *721*....25
17. Stator flux ripple corresponding to bus clamping sequences *0121*, *7212*, *1012* and *2721*....26
18. Block diagram of the DSP based experimental setup. 30
19. Comparison of sequences *0121* and *7212*....31
20. Comparison of sequences *0127*, *0121* and *7212*....31
21. Three zone hybrid PWM technique I. 32
22. Measured spectra of PWM waveforms (line-line) corresponding to conventional SVPWM and 3-Zone hybrid PWM I, at a fundamental frequency of 60 Hz....33
23. Measured spectra of PWM waveforms (line-line) corresponding to conventional SVPWM and 3-Zone hybrid PWM I, at a fundamental frequency of 60 Hz....33
24. No-load current waveforms corresponding to conventional SVPWM and 3-Zone hybrid PWM I. 34

25. Analytical results of V_{WTHD} vs. frequency for conventional SVPWM and 3-Zone hybrid PWM I. 35
26. Experimental results of I_{THD} vs. frequency for conventional SVPWM and 3-Zone hybrid PWM I. 35
27. Three zone hybrid PWM technique II shown in the space vector plane. 36
28. Five-zone hybrid PWM technique. 36
29. Analytical results of V_{WTHD} vs. frequency for CSVPWM and five-zone hybrid PWM. 37
30. Experimental results of I_{THD} vs. frequency for CSVPWM and five-zone hybrid PWM. 37
31. Measured spectra of PWM waveforms (line-line) corresponding to CSVPWM and Five-Zone hybrid PWM, at a fundamental frequency of 60 Hz. 37
32. No-load current waveforms corresponding Five-Zone hybrid PWM. 38
33. Seven-zone hybrid PWM technique. 38
34. Analytical results of V_{WTHD} vs. frequency for seven-zone hybrid PWM. 39
35. Experimental results of I_{THD} vs. frequency for Seven-Zone hybrid PWM. 39
36. Measured spectra of PWM waveforms (line-line) corresponding to CSVPWM and seven-zone hybrid PWM, at a fundamental frequency of 60 Hz. 39
37. No-load current waveforms of CSVPWM and seven-zone hybrid PWM 40
38. Comparison of the three THD-based hybrid techniques with CSVPWM in terms of analytical V_{WTHD} vs. frequency. 40
39. Comparison of the three THD-based hybrid techniques with CSVPWM in terms of experimental I_{THD} vs. frequency. 40
40. Switching loss factor over a fundamental period for phase 'a' corresponding to different sequences at power factor angle of 30^0. 45
41. Total switching loss in phase 'a' for different sequences normalized to switching loss corresponding to CSVPWM. 46
42. Switching loss optimized PWM in the α–ϕ plane 48
43. Normalized switching loss of the switching loss optimized hybrid PWM technique. 48

44. Experimental PWM waveforms and line currents corresponding to CSVPWM and switching-loss-optimized PWM....50
45. Comparison of conventional SVPWM, THD-optimized-PWM (seven-zone) and switching-loss-optimized-PWM in terms of THD and switching loss....52
46. Zones of superior performance in terms of quality factor at a fundamental frequency of 60Hz....54
47. Simulation results comparing the quality factor for CSVPWM with the hybrid PWM suggested in Fig. 46....54
48. Four different hybrid PWM techniques to simultaneously reduce THD and switching loss....56
49. Simulation results comparing THD and switching loss corresponding to the four new combined hybrid PWM techniques with those of CSVPWM....57
50. Experimental PWM waveforms and line currents for CSVPWM and Type I and Type IV hybrid PWM techniques at 50 Hz and at a power factor angle of 30^0 lagging....58
51. Hybrid PWM technique utilizing instantaneous current feedback....60
52. Simulation results comparing CSVPWM with PWM technique of Fig. 51....61
53. Hybrid PWM technique using power factor angle and instantaneous current feedback....62
54. Simulation results comparing CSVPWM with PWM technique of Fig. 53....63
55. Experimental PWM and line current waveforms corresponding to CSVPWM and hybrid PWM technique shown in Fig. 53 at different power factor angles....64

1. INTRODUCTION

1.1 Motivation and Objectives of the Research Project

Three-phase voltage source inverter (VSI) fed induction motors are popularly used as variable speed drives. Extensive research has been carried out on pulse-width modulation (PWM) techniques for VSI fed drives [1-18]. Triangle-comparison approach and space vector approach have been the two most popular approaches to real-time PWM generation. The two approaches were held to be equivalent [4,10,11]. However, recent research has indicated that the space vector approach offers additional degrees of freedom in designing PWM techniques over the classical triangle-comparison methods [17,18].

The main objectives of the research described in this report are as follows:

1. Systematic study on the additional degrees of freedom available in the space vector approach, using new sequences, which are not possible in the triangle-comparison methods.
2. Analysis of the impact of the new sequences, which permit the additional degrees of freedom, on the distortion in motor line currents and on the switching losses of the inverter.
3. Design and experimentally demonstrate new hybrid PWM techniques using the above sequences to simultaneously reduce both the line current distortion and switching losses.

1.2 Popular PWM Techniques

A voltage source inverter is used to apply variable magnitude, variable frequency three-phase AC voltage to the motor to control its speed as shown in Fig. 1. A block diagram of a VSI fed drive is shown in Fig. 2. Note that the controller and pulse width modulator are shown explicitly as two different blocks. The controller determines the dynamic performance of the drive. For example, vector control is used in applications where high dynamic performance is required, whereas V/F control is used where the transient response is not of importance. The controller provides the voltage reference for the modulator (PWM).

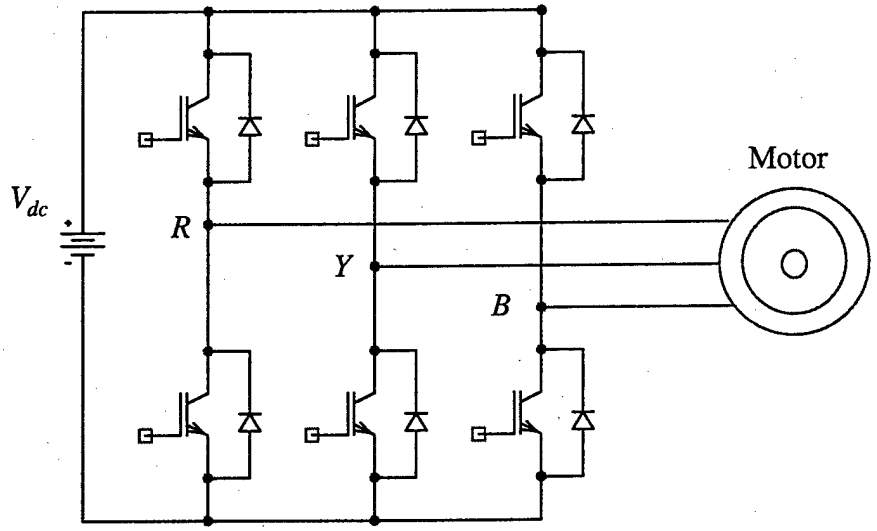

Fig. 1. Three-phase voltage source inverter for motor drives

The modulator determines the switching instants of the devices in the three-phase bridge based on the voltage reference, and optionally, on the motor currents also. The calculated switching instants are such that the applied voltage on the motor equals the commanded reference voltage in an *average sense*. The modulator affects the steady-state performance including efficiency and total harmonic distortion factor (THD). The present work aims at enhancing the steady-state performance, both in terms of efficiency and waveform quality, without compromising on the dynamic performance.

Triangle comparison method and the space vector PWM method are the two most popular approaches to real time PWM generation.

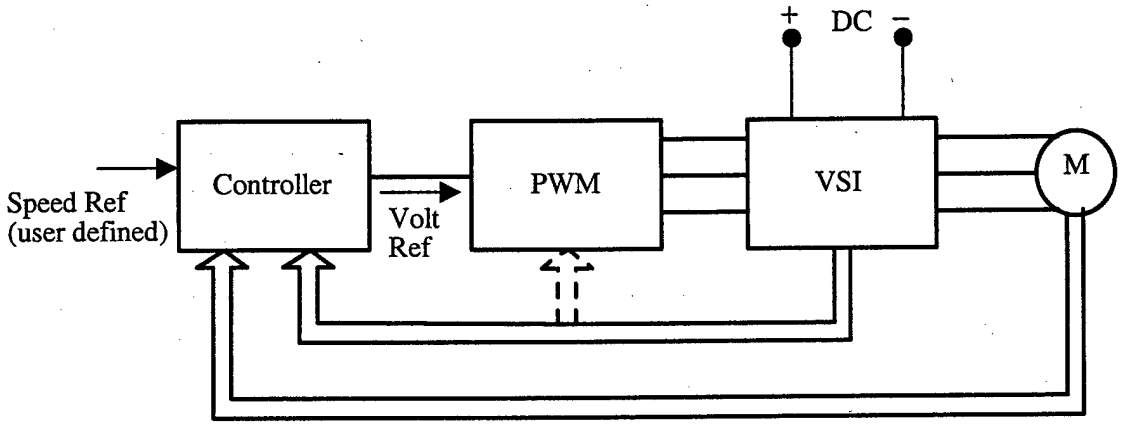

Fig. 2. Block diagram of a voltage source inverter fed AC motor drive

Triangle-Comparison Approach

Triangle-comparison approach, such as sine-triangle PWM, involves comparison of three phase modulating waves against a common triangular carrier to determine the switching instants of the three phases. It is also referred to as 'per-phase' approach, since there is a distinct modulating wave corresponding to each of the phases.

Fig. 3 shows some of the popularly used modulating waveforms (shown just for one phase). SPWM corresponds to the conventional sinusoidal PWM and SV-PWM corresponds to a modulating wave that gives similar performance as that of conventional space vector modulation described in the next section. In the modulating wave referred to as 'Bus-clamped', the instantaneous value of the modulating wave equals the peak of the carrier for one third of every half cycle. Therefore, the corresponding phase does not switch, or is clamped, for one third of the half cycle. Such bus-clamping PWM techniques reduce the average switching frequency of the devices to two-thirds the carrier frequency [7], and therefore, lower the switching losses.

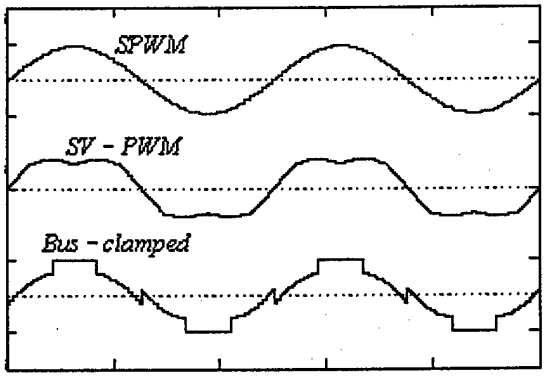

Fig. 3. Different modulating waves used in triangle-comparison approach

Space Vector Approach

The three-phase inverter, shown in Fig. 1, has eight switching states – six active states and two zero states. The six active states lead to corresponding active voltage vectors as shown in Fig. 4. These active vectors divide the space vector plane into six sectors as shown. The two zero states lead to a zero voltage vector.

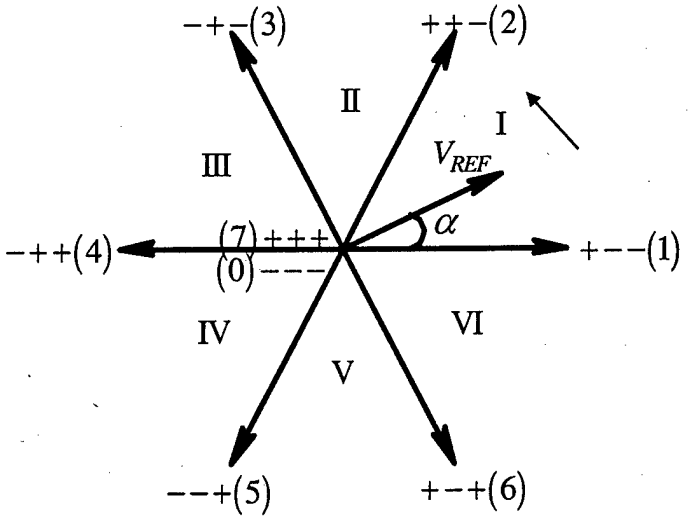

Fig. 4. Switching states and corresponding voltage vectors of a voltage source converter

The reference vector has a constant magnitude and revolves with a constant frequency at steady state as shown in Fig. 4. A fundamental cycle is divided into several small sub-cycles. The reference is sampled once in every sub-cycle. An average vector, equal to the sampled reference vector, is generated by time averaging the voltage vectors produced by the inverter over the given sub-cycle. Given a commanded vector with magnitude V_{REF} and spatial angle α in sector I as shown in Fig. 4, the volt-second balance is maintained over the given sub cycle as follows.

$$V_{REF}\angle\alpha \times T_S = 1\angle 0^o \times T_1 + 1\angle 60^o \times T_2 + 0 \times T_Z \qquad \ldots. \qquad (1)$$

where, $T_1 = V_{REF}\dfrac{sin\left(60^o - \alpha\right)}{sin 60^o} T_S$

$$T_2 = V_{REF}\frac{sin(\alpha)}{sin 60^o} T_S$$

$$T_Z = T_S - T_1 - T_2$$

The active state *1*, the active state *2* and the two zero states together are applied for durations T_1, T_2 and T_Z, respectively, as shown in (1).

In the conventional space vector PWM, T_Z is divided equally between the two zero states. In modified space vector PWM, or bus clamping space vector PWM, only one zero state is applied for the entire T_Z [4,10].

Fig. 5 shows the variation of THD with modulation index for different PWM techniques. Bus clamping PWM techniques reduce the average switching frequency, resulting in lower switching losses. However, the harmonic distortion is increased, as shown in Fig. 5.

Much of the research on space vector PWM has focused on optimal division of the zero state duration leading to different types of bus-clamping PWM. The conventional, as well as the above-mentioned modified forms of space vector PWM, are equivalent to the triangle comparison approach [4,10]. However, recently it has been shown that the space vector approach offers additional flexibilities over the triangle-comparison approach in the design of PWM techniques, when division of active state duration is also introduced [17,18].

The division of active state duration in a subcycle introduces several new sequences in the implementation of space vector PWM. In this research these new sequences are systematically studied in terms of their effect on THD and switching

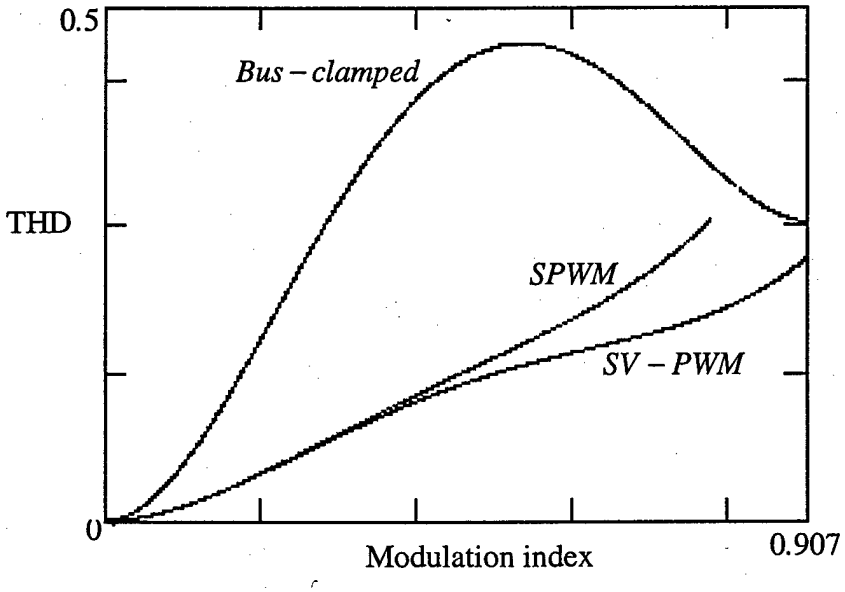

Fig. 5. Variation of THD with modulation index for different PWM techniques

losses. Based on this study, new hybrid PWM techniques that involve using different sequences in different subcycles within a sector are developed, with the objective of achieving simultaneous reduction in THD and switching losses.

2. NEW SEQUENCES INVOLVING DIVISION OF ACTIVE STATE DURATION

2.1 Derivation of All Possible Sequences

As discussed in the previous section, the reference vector is sampled once in every subcycle, T_S and an average voltage vector equal to the sampled reference vector is generated by time averaging the nearest active vectors and zero vectors. When the sample of the reference vector falls in sector I as shown in Fig. 4, the durations for which active vector *1*, the active vector *2* and the zero vector are to be applied for volt-second balance are given by (1). Since the six sectors are symmetric, it is sufficient to analyze Sector I alone.

Though the three voltage vectors must be applied exactly for durations given in (1), they can be applied in different *sequences* within a subcycle. The multiplicity of switching sequences can primarily be attributed to two factors: Firstly, the zero vector can be applied either using the zero state *0* or the zero state *7*. The division of T_Z between the two zero states has been thoroughly investigated [7,11]. Secondly, a given active vector need not be applied continually for the total required duration. For example, the active vector *1* can be applied over two intervals of time within the subcycle adding up to T_1. This multiple application of an active vector within a subcycle [17,18] has received very little attention so far, and is a major focus of the research reported here.

The choice in the division of zero states leads to three different sequences, which are presently widely used. These sequences are illustrated in Fig. 6. Conventional space vector PWM (CSVPWM) divides the zero vector time T_Z equally between the two zero states *0* and *7* in every subcycle. Conventional sequence *0127* is illustrated in Fig. 6a. It

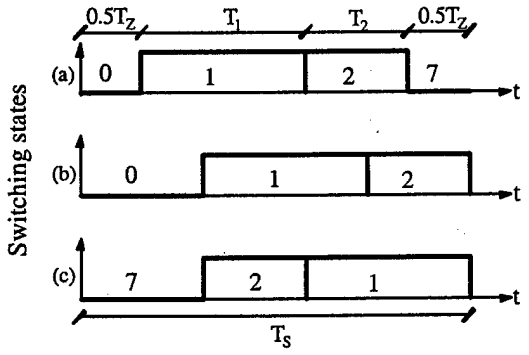

Fig. 6. Conventional and existing bus-clamping sequences

should be noted that in the interest of reducing the number of switchings, the same vector that is used at the end of a subcycle is also used at the start of the subsequent subcycle. Therefore, for example, sequence *0127* in further discussion, actually refers to the application of space vectors in the following sequence – *0127, 7210, 0127, 7210...* The reverse sequence is not shown explicitly.

Existing bus-clamping PWM techniques employ clamping sequences, which use only one zero state for the entire duration T_Z in a subcycle. The known clamping sequences *012* and *721* are shown in Figs. 6b and 6c, respectively. Use of *012* where the zero state *0* alone is used in a subcycle, results in phase 'c' being clamped to the negative DC bus during the entire subcycle. Use of *721*, where the zero state *7* alone is applied leads to clamping of phase 'a' to the positive DC bus during the subcycle. As either of the two phases can be clamped by avoiding one of the two zero states, these two phases can be termed as the 'clampable phases' of sector I.

The conventional sequence *0127* results in a total of three switchings – each phase switching once, in a subcycle. The bus clamping sequences results in only two switchings per subcycle. Also, all the above sequences involve switching of only one phase during a transition from one state to another. Therefore, while deriving all the possible sequences, with the newly added freedom of dividing the active state duration, the following constraints must be satisfied (apart from satisfying volt-second balance).

1. Only one phase switches during any state transition. For example, transition from state *0* to state *1* and vice versa involves switching of phase 'a' alone and hence is allowed. But, transition from state *0* to state *2* is not allowed, since it involves switching of both phase 'a' and phase 'b' during the transition.
2. The total number of switchings in all the phases per subcycle should be less than or equal to three.
3. The same state at the end of a subcycle should be used at the start of the next subcycle.

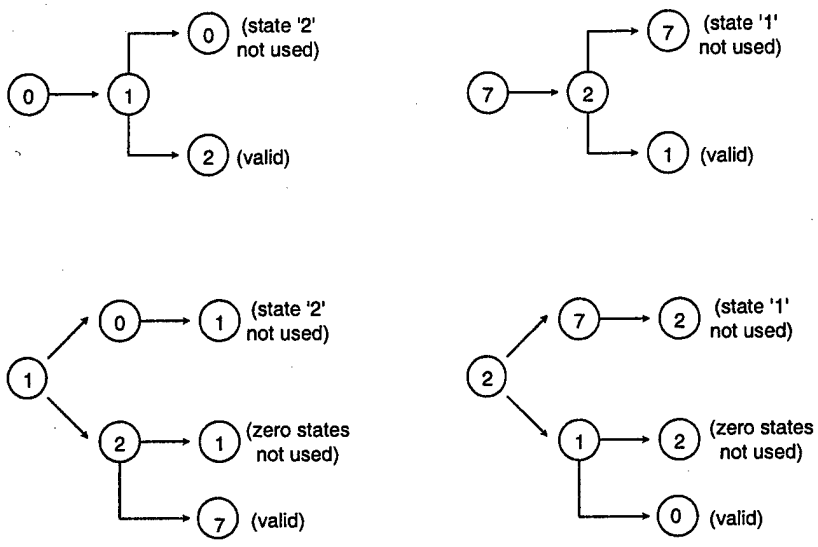

Fig. 7. Derivation of possible sequences that result in two switchings in a sub-cycle

Fig. 7 shows the derivation of all possible sequences that have only two switchings per subcycle and satisfy the above constraints. As seen, these are the known bus-clamping

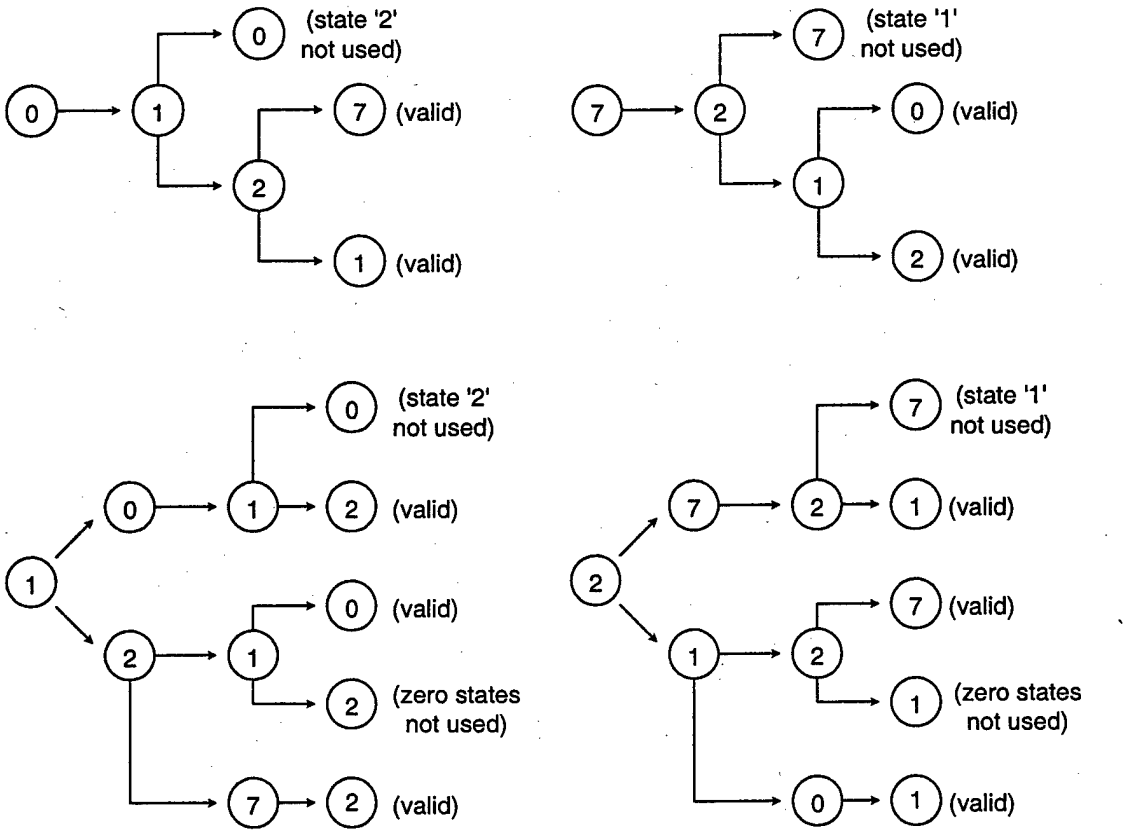

Fig. 8. Derivation of possible sequences that result in three switchings in a sub-cycle

sequences *012* and *217*. Note that the other two valid sequences are only the reverse sequences of the above two, and hence are not considered as new sequences. It may also be observed that with only two switchings per subcycle, sequences that involve division of active state duration are not possible.

Fig. 8 shows the derivation of all possible sequences that have three switchings per subcycle and satisfy the above constraints. For example, starting from state *0* in Fig. 8a, the only possibility for the next state is *1*, since states *2* or *7* will involve multiple switchings. From state *1*, though transition to state *0* is possible, it will rule out the use of state *2*, and hence is not a valid sequence. Therefore the next state has to be *2*. From state *2*, transitions to either state *1* or state *7* involve only one switching and hence both are allowed. This leads to two sequences – the conventional sequence *0127* and the new sequence *0121*, which involves division of the duration of active state *1*. Following a similar procedure all the possible sequences with the above mentioned constraints can be derived as illustrated in Fig. 8.

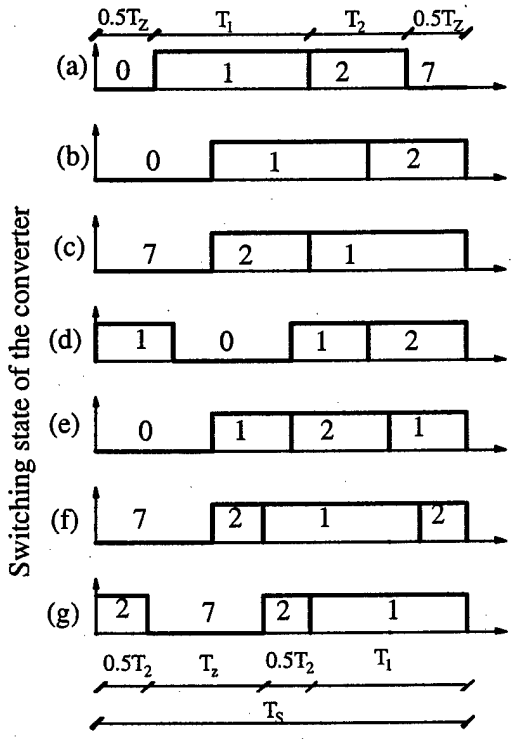

Fig. 9. All possible sequences satisfying the imposed constraints

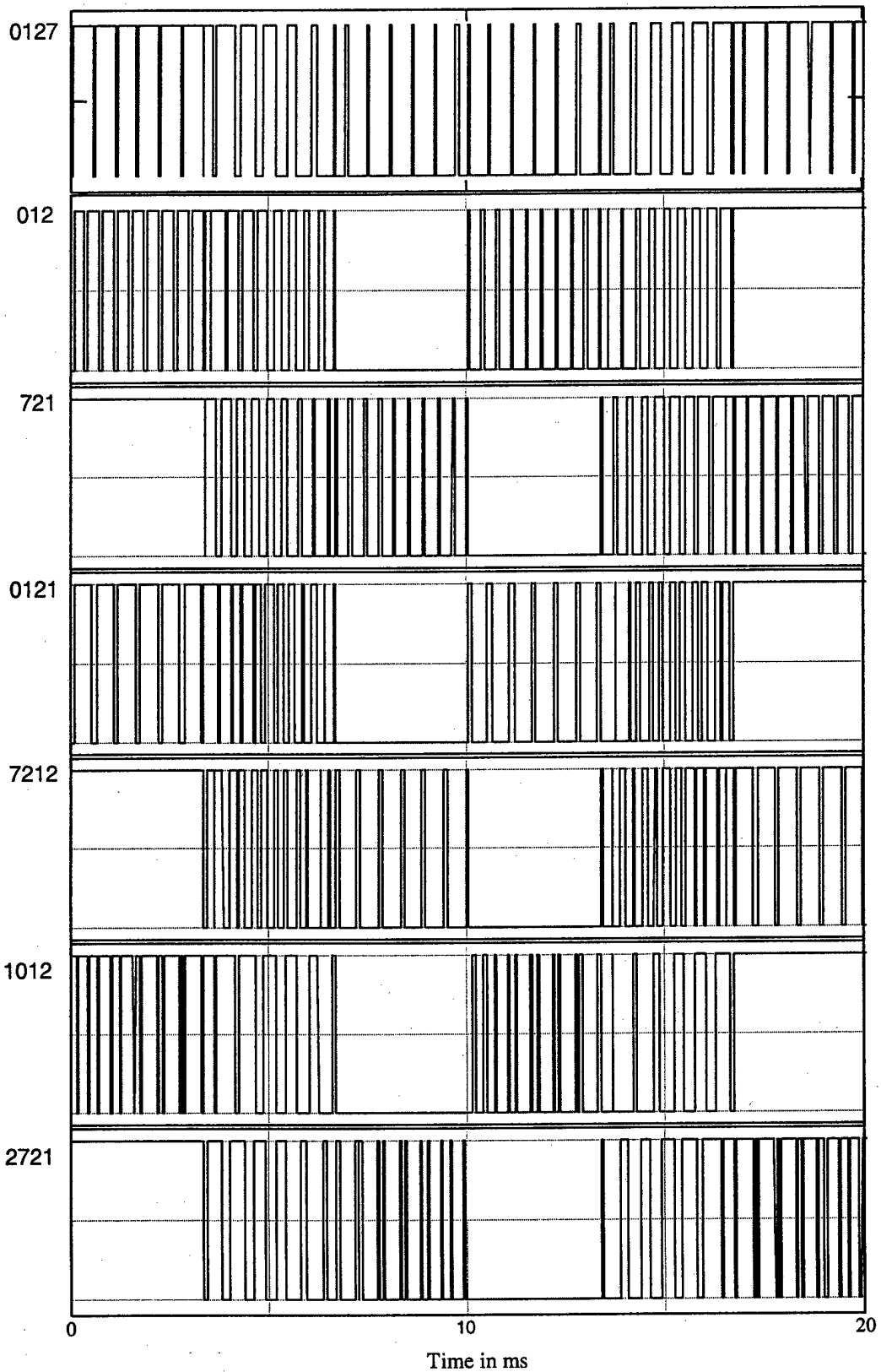

Fig. 10. PWM waveforms corresponding to each of the seven sequences at a fundamental frequency of 50 Hz and an average switching frequency of 1 kHz

Fig. 9 shows the seven possible sequences that can be used in space vector

approach satisfying the imposed constraints. The last four are new sequences that involve division of active state duration. It may be noted that in Fig. 9, whenever there is a division of the duration of a state, either active or zero state, it is divided into two equal intervals. It is possible to divide the durations unequally also, but this is beyond the scope of this research project, and may be pursued in the future. The PWM waveforms generated by each of the seven sequences are shown in Fig. 10.

2.2 Distinguishing Features of Sequences Involving Active State Division

The PWM waveforms obtained using conventional space vector PWM using sequence *0127* and the different types of bus-clamping space vector PWM using sequences *012* and *721* can be equivalently obtained using the triangle comparison approach. Corresponding to each of the sequences above, there exists a suitable modulating wave with an appropriate triplen harmonic added, which when compared with a fixed frequency, uniform, triangular carrier wave can result in identical PWM waveforms as that of the space vector approach. However, there is no such equivalence in the triangle comparison approach for sequences *0121, 1012, 7212* or *2721* that involve division of active state duration. In sine-triangle PWM and conventional space vector PWM every phase switches once in every sub-cycle (or equivalently, every half carrier cycle). In bus clamping PWM, two phases switch once each, while the third phase is clamped in every sub-cycle. Thus, in state of the art PWM techniques, no phase switches more than once in a sub-cycle. In other words, no switching state is applied more than once in a sub-cycle

The most distinguishing feature of the new sequences is that they involve *multiple switchings of a phase* within a sub-cycle, while clamping another phase to one of the dc rails. For example, *1012* results in double switching of phase 'a' (transition from *1* to *0*, and again from *0* to *1*), single switching of phase 'b' and clamping of phase 'c' to the negative bus in a given sub-cycle in Sector I. Table I gives the number of switchings of each phase in a sub-cycle in Sector I corresponding to all the seven possible sequences. Note that the total number of switchings in all the sequences is less than or equal to three.

TABLE I

NUMBER OF SWITCHING IN EACH PHASE IN SECTOR I FOR ALL SEQUENCES

No.	Number of switching			Sequences	Remarks
	Phase 'a'	Phase 'b'	Phase 'c'		
1	1	1	1	0127-7210	Conventional
2	1	1	0	012-210	Bus clamping
3	0	1	1	721-127	Bus clamping
4	2	1	0	1012-2101	New
5	1	2	0	0121-1210	New
6	0	2	1	7212-2127	New
7	0	1	2	2721-1272	New

Due to multiple switchings of a phase within a subcycle, space vector PWM with new sequences does not have an equivalence in the per-phase or triangle comparison approach. The corresponding PWM waveforms cannot be generated by comparing any

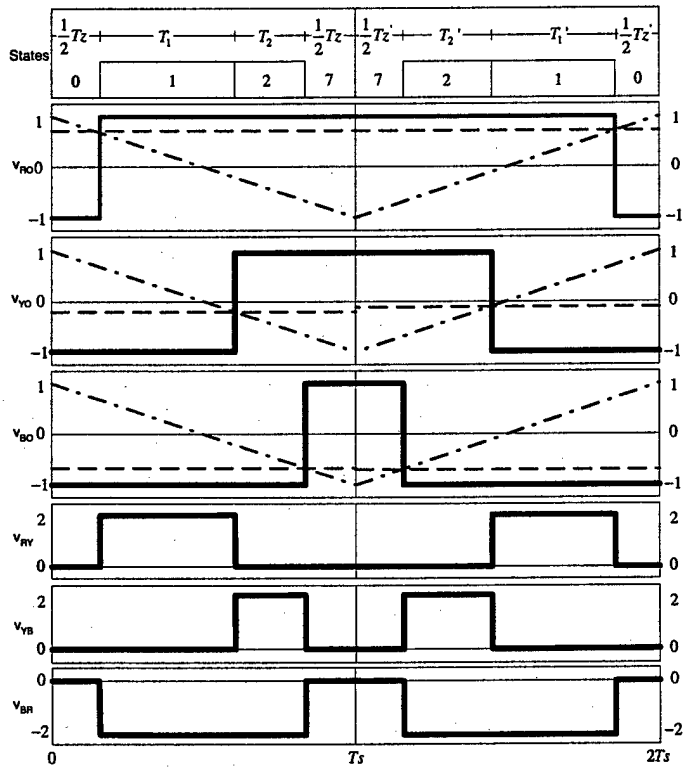

Fig. 11. Generation of PWM corresponding to *0127* using triangle comparison approach

modulating wave with a fixed frequency, common triangular carrier. It may be possible to generate these waveforms using different carrier waves for different phases, whose frequency as well as shape change at different points in the fundamental cycle. Fig. 11 shows the generation of PWM waveforms corresponding to conventional sequence *0127* using the triangle comparison approach. As seen, the three pole voltages can be generated by comparing three-phase sinusoidal voltages with a common triangular carrier. Fig. 11 also shows the three line-line voltages, corresponding to *0127*. As seen, the line-line voltages have a total of two pulses in two sub-cycles.

Similarly, Fig. 12 shows the generation of PWM waveforms corresponding to the bus-clamping sequence, *012*, where phase 'c' is clamped. Again, the pole voltages can be equivalently generated by comparing suitable modulating waves with a common, uniform triangular carrier. Fig. 12 also shows the line-line voltages. As seen, one of the line-line voltages have two pulses in two sub-cycles while the other two phases have only one pulse in two cycles.

Fig. 13 illustrates an attempt to generate PWM waveforms identical to those generated by the new sequence *0121*, using triangle comparison approach. As seen, the

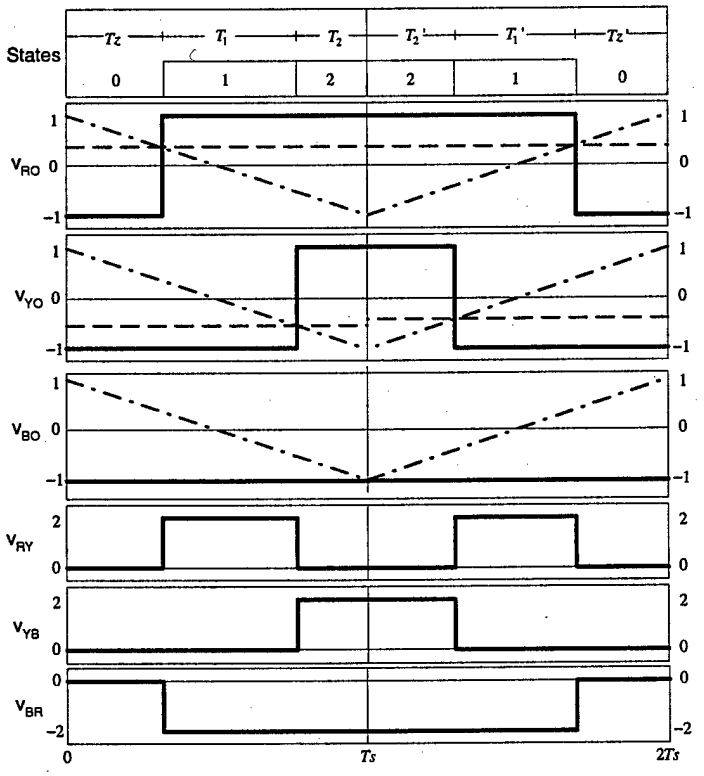

Fig. 12. Generation of PWM corresponding to *012* using triangle comparison approach

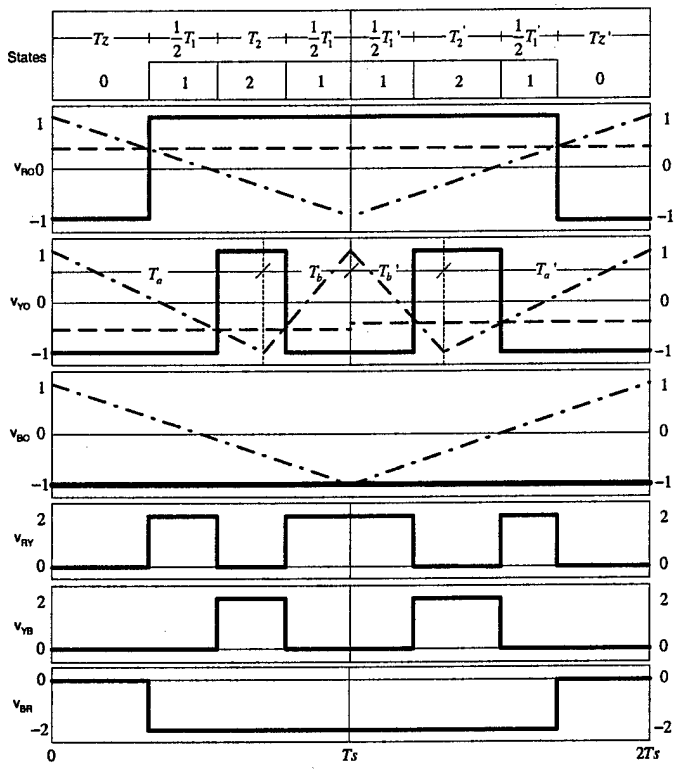

Fig. 13. Generation of PWM corresponding to *0121* using triangle comparison approach. Note that a complex carrier wave is required.

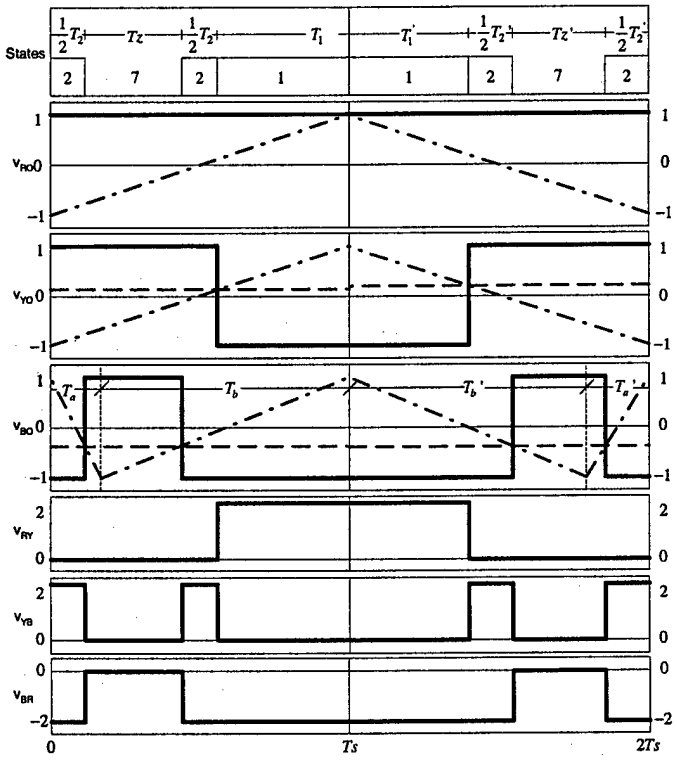

Fig. 14. Generation of PWM corresponding to *2721* using triangle comparison approach. Note that a complex carrier wave is required.

carrier wave for phase 'b', which double switches, needs to be at twice the frequency

compared to that of other two phases, at selected points. Therefore, the carrier waves have to be different for each of the three phases, and for each carrier wave the frequency is different at different instants in a fundamental period. The waveform of the required carrier also depends on V_{REF}. Clearly, such a carrier waveform is very difficult to generate. The line-line voltages corresponding to *0121* are also shown in Fig. 13. As seen, the three line-line voltages have different pulses per sub-cycle. V_{ab} has three pulses in two sub-cycles, V_{bc} two pulses in two sub-cycles and V_{ca} only one pulse in two sub-cycles. Similarly, waveforms corresponding to the new sequence *7212* are shown in Fig. 14. Again, a very complex carrier wave is required to generate the PWM waveforms by an equivalent triangle comparison approach.

The above discussion clearly indicates that the space vector approach to generation of PWM waveforms is a more general approach than the per-phase approach, and the sequences that divide active state durations fully exploit the additional degrees of freedom offered by the space vector approach. As will be explained in later sections, the double switchings of a phase leads to PWM waveforms with lower THD. By properly choosing the sequences such that a phase whose instantaneous current is near zero crossing double switches, while the phase whose current is at or near its peak value is clamped, the switching losses can also reduced.

3. THD CHARACTERISTICS OF NEW SEQUENCES

A major performance measure of PWM techniques is the distortion in the line current. Evaluation of different techniques is often done based on the spectral properties of the PWM waveforms. Fourier analysis, Fourier theory of jumps (FTJ) [19] and double Fourier series (DFS) can be used to determine the harmonic content of different types of PWM waveforms [20]. Closed form expressions for harmonic components of PWM waveforms generated by triangle comparison approaches and conventional space vector PWM have been derived using FTJ and DFS methods [19,20]. However, it is convenient to compare PWM techniques directly based on the distortion in the line current waveform rather than the individual voltage harmonic components. The total harmonic distortion of the no-load current waveform, I_{THD}, defined in (2) is a widely used performance index for the quality of the waveform generated. I_1 and I_n in (2) are the RMS values of the fundamental and the nth harmonic components of the no-load current, respectively.

$$I_{THD} = \frac{1}{I_1}\sqrt{\sum_{n\neq 1} I_n^2} \qquad \ldots \qquad (2)$$

The weighted total harmonic distortion factor of the line voltage, V_{THD}, defined in (3) is equivalent to I_{THD} and is independent of the motor parameters [1]. V_1 and V_n are the RMS values of the fundamental and nth harmonic components of the line-line voltage, respectively.

$$V_{THD} = \frac{1}{V_1}\sqrt{\sum_{n\neq 1}\left(\frac{V_n}{n}\right)^2} \qquad \ldots \qquad (3)$$

Therefore, V_{THD} can be determined from the individual harmonic components obtained using any of the frequency domain methods. Alternatively, the quality of line current waveform can be directly determined in time domain by integrating the error voltage. In this work, a time domain analysis method based on the notion of *stator flux ripple* is used to estimate current ripple at a sub-cycle level, which is subsequently integrated over a fundamental cycle. This generalized method of analysis can be applied for conventional sequences as well as new sequences that involve division of active state duration.

3.1 Analysis Based on Stator Flux Ripple

The applied voltage vector equals the reference voltage vector only in an average sense over the given subcycle, and not in an instantaneous fashion. The difference between the reference vector and the instantaneous applied voltage vector is the instantaneous error voltage vector. The time integral of the error voltage vector, is referred to as the 'stator flux ripple vector', and is a measure of the ripple in the line current.

At any instant within a given subcycle, one of the two active vectors or the zero vector is applied. When the zero vector is applied, the error voltage vector is equal to the negative of the average vector to be generated. When an active vector is applied, the error voltage vector is the vector originating from the tip of the average vector and ending at the tip of the active vector applied. Volt-second balance ensures that the stator flux ripple vector starts and ends with zero magnitude in every subcycle. Fig. 14 shows the trajectory of the stator flux ripple corresponding to the conventional sequence *0127*, for a given V_{REF} and spatial angle, α.

The error vector can be resolved in a synchronously revolving d-q reference frame, which is useful while comparing different sequences. The d-axis and the q-axis components of the stator flux ripple vector corresponding to *0127* are shown in Fig. 15. The values of q-axis ripple at the switching instants are given in terms of Q_Z, $Q1$ and Q_2, while those of d-axis ripple are given in terms of D. The quantities Q_Z, Q_1, Q_2 and D are defined in (4).

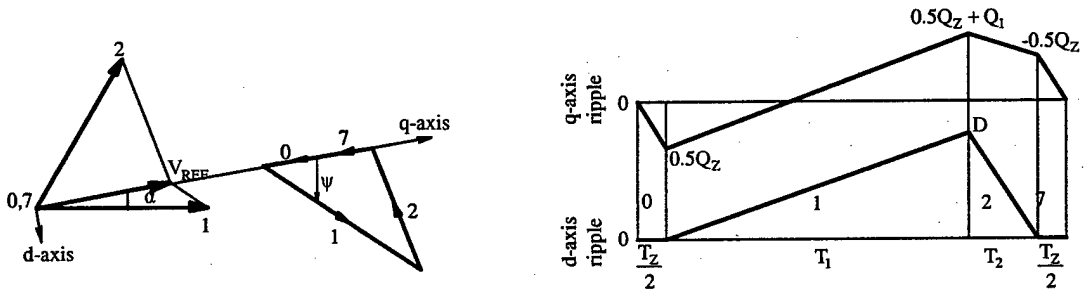

Fig. 15. Stator flux ripple corresponding to *0127*

$$
\begin{aligned}
Q_Z &= -V_{REF} T_Z \\
Q_1 &= [\cos(\alpha) - V_{REF}]\, T_1 \\
Q_2 &= \left[\cos(60^\circ - \alpha) - V_{REF}\right] T_2 \\
D &= \sin(\alpha)\, T_1
\end{aligned}
\qquad \ldots \qquad (4)
$$

The mean square value of the stator flux ripple vector gives a measure of the distortion in the line currents. From Fig. 15, the expression for mean square ripple, F_{0127}^2 over a sub-cycle for sequence *0127* can be obtained as shown in (5).

$$
\begin{aligned}
F_{0127}^2 = {} & \frac{1}{3}(0.5Q_Z)^2 \frac{T_Z}{2T_S} + \frac{1}{3}\left[\begin{matrix}(0.5Q_Z)^2 + 0.5Q_Z(0.5Q_Z + Q_1) \\ +(0.5Q_Z + Q_1)^2\end{matrix}\right]\frac{T_1}{T_S} \\
& + \frac{1}{3}\left[(0.5Q_Z + Q_1)^2 - (0.5Q_Z + Q_1)0.5Q_Z + (-0.5Q_Z)^2\right]\frac{T_2}{T_S} \\
& + \frac{1}{3}(-0.5Q_Z)^2 \frac{T_Z}{2T_S} + \frac{1}{3}D^2 \frac{(T_1 + T_2)}{T_S}
\end{aligned}
\qquad \ldots \qquad (5)
$$

Similarly the stator flux ripple corresponding to the known bus-clamping sequences, *012* and *721*along with their q-axis and d-axis components are shown in Figs. 16a and 16b respectively. Same values of V_{REF} and α have been assumed for all sequences. However, the subcycle duration considered for a sequence is in proportion to the number of switchings per subcycle to enable a comparison of the different sequences at a given average switching frequency (F_{SW}). Expressions for the mean square value of the stator flux ripple vector for *012* and *721* can be derived from Fig. 16 and are given in (6) and (7) respectively.

$$
\begin{aligned}
F_{012}^2 = {} & \frac{1}{3}Q_Z^2 \frac{T_Z}{T_S} + \frac{1}{3}\left[Q_Z^2 + Q_Z(Q_Z + Q_1) + (Q_Z + Q_1)^2\right]\frac{T_1}{T_S} \\
& + \frac{1}{3}\left[(Q_Z + Q_1)^2\right]\frac{T_2}{T_S} + \frac{1}{3}D^2 \frac{(T_1 + T_2)}{T_S}
\end{aligned}
\qquad \ldots \qquad (6)
$$

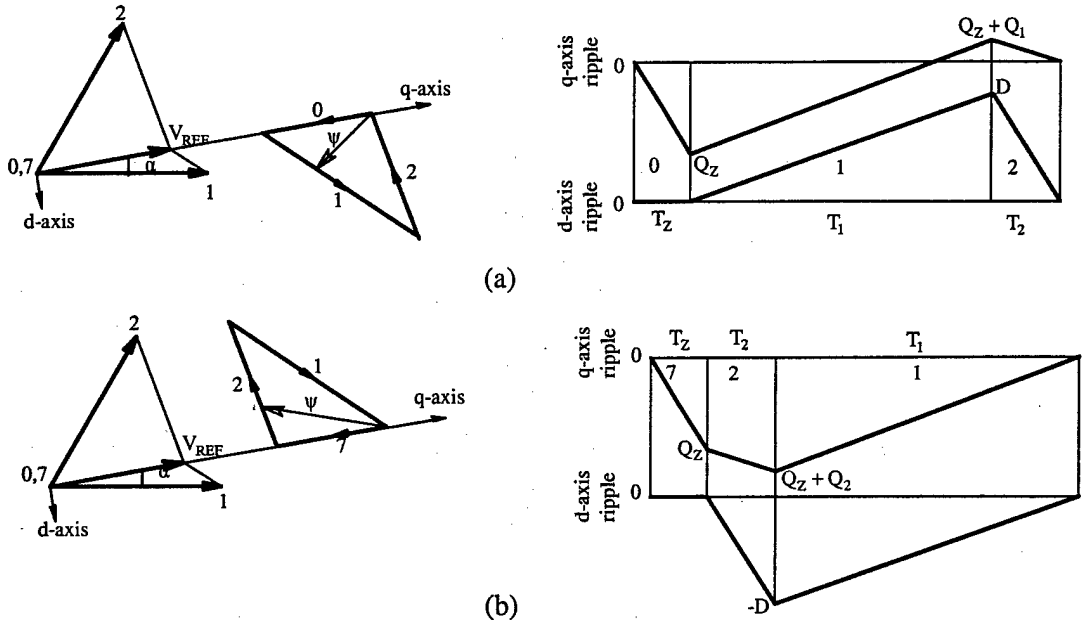

Fig. 16. Stator flux ripple corresponding to sequences (a) 012 and (b) 721

$$F_{721}^2 = \frac{1}{3}Q_Z^2\frac{T_Z}{T_S} + \frac{1}{3}\left[Q_Z^2 + Q_Z(Q_Z+Q_2) + (Q_Z+Q_2)^2\right]\frac{T_2}{T_S} + \frac{1}{3}\left[(Q_Z+Q_2)^2\right]\frac{T_1}{T_S} + \frac{1}{3}D^2\frac{(T_1+T_2)}{T_S} \quad \ldots \quad (7)$$

Finally, stator flux ripple corresponding to new sequences involving active state division, namely *0121*, *7212*, *1012* and *2721* along with their q-axis and d-axis components are shown in Fig. 17. Expressions for the mean square value of the stator flux ripple vector for each of these sequences can be derived from Fig. 17 and are given in (8) – (11).

$$F_{0121}^2 = \frac{1}{3}Q_Z^2\frac{T_Z}{T_S} + \frac{1}{3}\left[Q_Z^2 + Q_Z(Q_Z+0.5Q_1) + (Q_Z+0.5Q_1)^2\right]\frac{T_1}{2T_S} + \frac{1}{3}\left[(Q_Z+0.5Q_1)^2 - (Q_Z+0.5Q_1)0.5Q_1 + (-0.5Q_1)^2\right]\frac{T_2}{T_S} + \frac{1}{3}(-0.5Q_1)^2\frac{T_1}{2T_S} + \frac{1}{3}(0.5D)^2\frac{(T_1+T_2)}{T_S} \quad \ldots \quad (8)$$

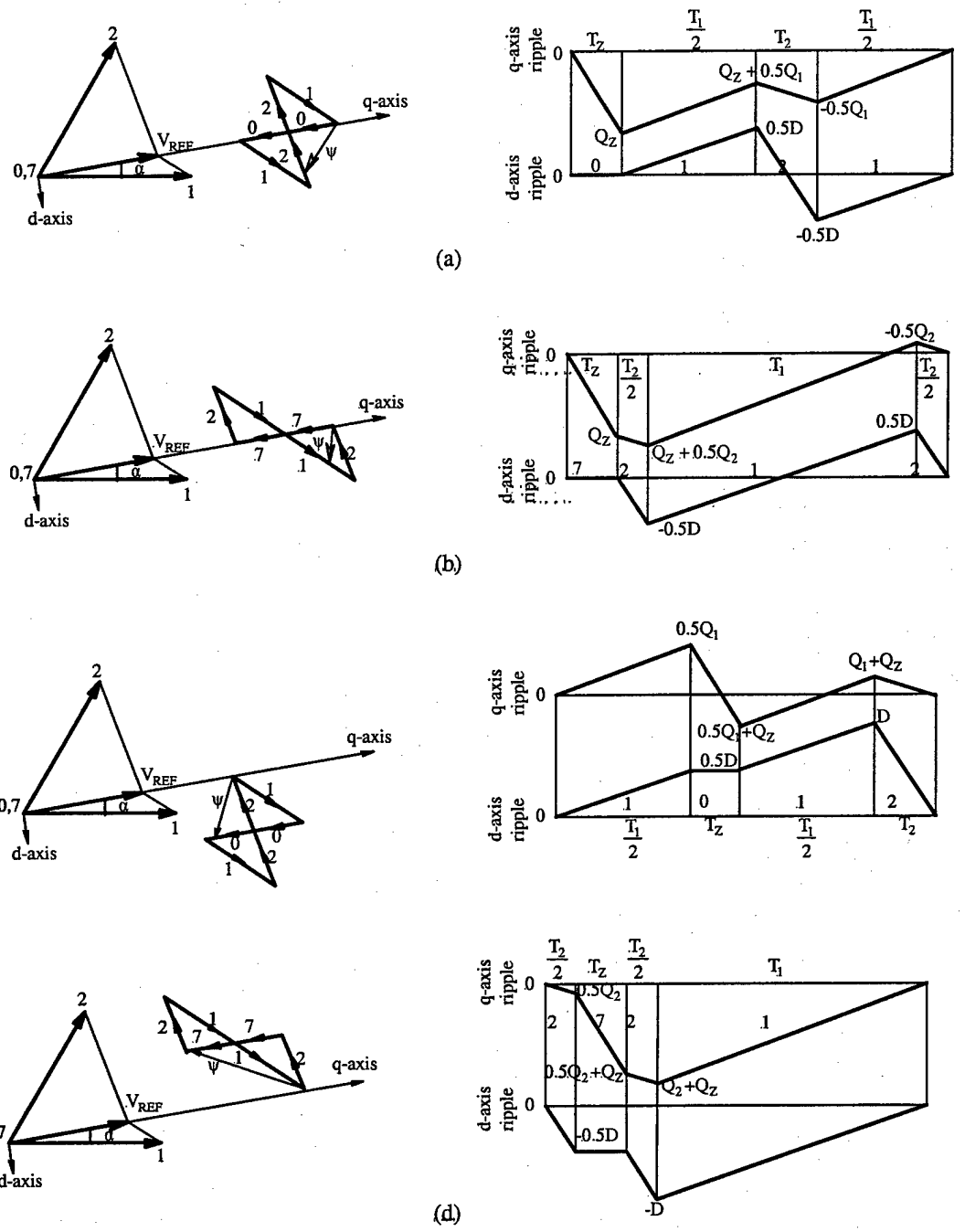

Fig. 17. Stator flux ripple corresponding to sequences (a) *0121*, (b) *7212*, (c) *1012* and (d) *2721*

$$F_{7212}^2 = \frac{1}{3}Q_Z^2\frac{T_Z}{T_S} + \frac{1}{3}\left[Q_Z^2 + Q_Z(Q_Z + 0.5Q_2) + (Q_Z + 0.5Q_2)^2\right]\frac{T_2}{2T_S}$$
$$+ \frac{1}{3}\left[(Q_Z + 0.5Q_2)^2 - (Q_Z + 0.5Q_2)0.5Q_2 + (-0.5Q_2)^2\right]\frac{T_1}{T_S} \quad \ldots \quad (9)$$
$$+ \frac{1}{3}(-0.5Q_2)^2\frac{T_2}{2T_S} + \frac{1}{3}(0.5D)^2\frac{(T_1+T_2)}{T_S}$$

$$F_{1012}^2 = \frac{1}{3}(0.5Q_1)^2\frac{T_1}{2T_S} + \frac{1}{3}\left[(0.5Q_1)^2 + 0.5Q_1(0.5Q_1+Q_Z) + (0.5Q_1+Q_Z)^2\right]\frac{T_Z}{T_S}$$
$$+\frac{1}{3}\left[(0.5Q_1+Q_Z)^2 + (0.5Q_1+Q_Z)(Q_1+Q_Z) + (Q_1+Q_Z)^2\right]\frac{T_1}{2T_S} \quad (10)$$
$$+\frac{1}{3}(Q_1+Q_Z)^2\frac{T_2}{T_S} + \frac{1}{3}D^2\frac{(T_1+T_2)}{T_S} + (0.5D)^2\frac{T_Z}{T_S}$$

$$F_{2721}^2 = \frac{1}{3}(0.5Q_2)^2\frac{T_2}{2T_S} + \frac{1}{3}\left[(0.5Q_2)^2 + 0.5Q_2(0.5Q_2+Q_Z) + (0.5Q_2+Q_Z)^2\right]\frac{T_Z}{T_S}$$
$$+\frac{1}{3}\left[(0.5Q_2+Q_Z)^2 + (0.5Q_2+Q_Z)(Q_2+Q_Z) + (Q_2+Q_Z)^2\right]\frac{T_2}{2T_S} \quad (11)$$
$$+\frac{1}{3}(Q_2+Q_Z)^2\frac{T_1}{T_S} + \frac{1}{3}D^2\frac{(T_1+T_2)}{T_S} + (0.5D)^2\frac{T_Z}{T_S}$$

The peak d-axis stator flux ripple for *0127* is *D* as shown in Fig. 15. Due to the reduced sub-cycle duration, the peak d-axis ripple for *012* and *721* reduces to 2*D*/3. The peak d-axis ripple due to sequences *0121* and *7212* is only half that of *0127* (i.e. *D*/2) as seen from Fig. 17. Correspondingly, the mean square d-axis ripple is also reduced as shown by the last terms in equations (8) and (9).

It can be inferred that more frequent switching of the 'unclampable phase' (or more frequent transitions between the active states) leads to reduction in d-axis ripple. At higher modulation indices, the d-axis ripple dominates over the q-axis ripple. Hence sequences *0121* and *7212* can be expected to result in least current ripple where the d-axis ripple is dominant, namely at high modulation indices, close to the maximum.

The above analysis based on stator flux ripple and the expressions for mean square ripple can be used to form new PWM techniques that involve new sequences. Two approaches to PWM generation using new sequences are investigated. In the first approach the same sequence (or symmetric pairs such as *0121* and *7212*, or *1012* and *2721*) are used throughout a sector. This leads to four different types of new bus-clamping PWM techniques that result in lower THD than the conventional bus clamping methods. The second approach is the hybrid PWM where, in each subinterval the sequence that results in the lowest mean square ripple is identified and applied.

4. HYBRID PWM TECHNIQUES TO REDUCE THD

Conventional space vector PWM uses the conventional sequence *0127* over the entire Sector I and corresponding sequences in other sectors. Similarly, bus-clamping PWM uses the clamping sequences through out. It may be noted that the same sequence need not be applied over the entire cycle. The choice of the sequence can be made in every sub-cycle. This choice need not be based only on the modulation index. It may also be based on the spatial angle of the reference vector. Also, the three-phase currents and other relevant variables may also be taken into account where necessary. The analytical study based on stator flux ripple described in the previous section can be used to make the optimum choice of sequence in a given sub-cycle, in terms of minimizing distortion in the line currents.

In this project, four different types of hybrid PWM techniques that minimize distortion in the line currents have been developed, by considering different sets of the possible seven sequences. The three-zone hybrid PWM technique uses the conventional sequence *0127* in conjunction with a pair of complementary sequences - either *0121* and *7212* or *1012* and *2721*. It may be noted that hybrid PWM technique involving *0127* and the bus clamping complementary pair – *012* and *217*, has already been investigated in the literature. The five-zone hybrid PWM technique uses the conventional sequence *0127*, and sequences *0121, 7212, 1012* and *2721*. All the five sequences included in this technique have the same number of switchings in a sub-cycle, and hence, the same sampling frequency. The final technique, namely, the seven-zone hybrid PWM, uses all the seven possible sequences. This technique involves twin-sampling frequency in order to maintain the average switching frequency the same as that of the other techniques.

4.1 General Procedure for the Design of Different PWM Techniques

The standard performance index used to compare different PWM techniques is the total harmonic distortion in the no-load line current, I_{THD} defined in (12).

$$I_{THD} = \frac{\sqrt{\sum I_n^{\,2}, n \neq 1}}{I_1} = \frac{\sqrt{I_{RMS}^{\,2} - I_1^{\,2}}}{I_1} \qquad \ldots \quad (12)$$

where I_{RMS} and I_n are the root mean square values of the no-load current waveform and the n^{th} harmonic current respectively, and I_1 is the root mean square value of the fundamental current under no-load. I_{THD} depends on the motor parameters like the leakage and the magnetizing inductances. An equivalent quantity, which is independent of the motor parameters, and gives a measure of I_{THD}, is the weighted harmonic distortion factor of the line-line voltage, V_{WTHD} defined in (3). The method based on stator flux ripple gives directly V_{WTHD}. In our analysis, simulation results will be based on V_{WTHD}, while the experimental results will be based on I_{THD}. The relationship between the two factors is given in (13).

$$V_{WTHD} = \frac{L_s}{L_{ls}} I_{THD} \qquad \ldots \qquad (13)$$
$$where, L_s = L_{ls} + L_m$$

where, L_m and L_{ls} are respectively the magnetizing inductance and the stator leakage inductance of the motor.

The general procedure for the design of hybrid PWM techniques, employing any given set of sequences, involves the following steps.

- Consider sub-cycle duration proportional to the number of switchings per sub-cycle for each sequence. (For example, $T_S = T$ for sequences with three switchings per sub-cycle, and $T_S = 2T/3$ for sequences with two switchings per sub-cycle.)
- Sketch the stator flux ripple trajectory over a sub-cycle for every sequence.
- Derive the expression for mean square ripple over a sub-cycle for every sequence.
- Identify the zone of superior performance for each sequence using the above expressions.

4.2 Experimental Setup

The experimental prototype consists of an IGBT based three-phase, two-level inverter driving a 2 hp induction motor from Baldor. The dc bus voltage is obtained by rectifying three-phase line voltage and has a nominal value of 325 V. The inverter is controlled by a digital signal processor, TMS320F243 from Texas Instruments, with a CPU clock frequency of 20 MHz. The studies were conducted at two different average inverter switching frequencies - 1.5 kHz and 3 kHz. Fig. 18 shows a block diagram of the experimental setup.

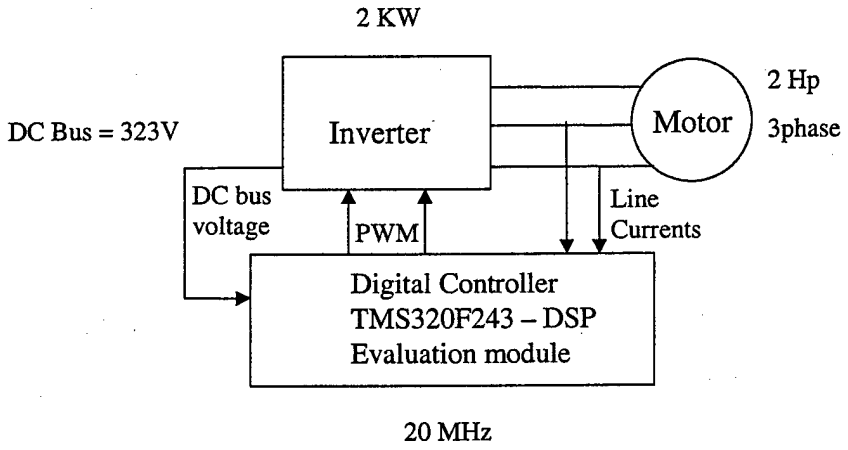

Fig. 18. Block diagram of the hardware prototype

4.3 Three-Zone Hybrid PWM Technique I: *0127, 0121* and *7212*

The first hybrid PWM technique denoted as three-zone hybrid PWM I, involves use of sequences *0127, 0121* and *7212*. The design of hybrid PWM technique for reduced current ripple involves determination of zones of superior performance for every sequence. The zone of superior performance for a given sequence is the spatial zone within a sector where the given sequence results in less RMS ripple than the other sequences considered.

The mean square ripple over a sub-cycle for any sequence is a function of V_{REF}, α and T_S. Since, all the three sequences considered in this technique involve three switchings per sub-cycle, the same sub-cycle duration, T_S, may be considered for all three sequences.

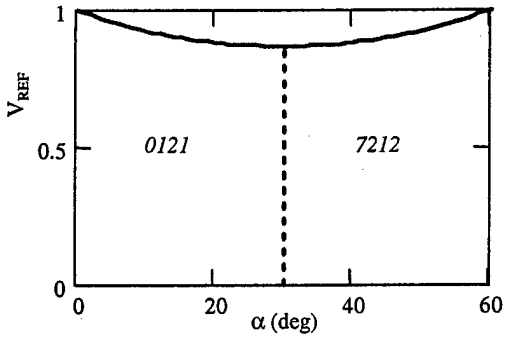

Fig. 19. Comparison of sequences *0121* and *7212* in terms of THD (zones of superior performance)

Comparison of 0121 and 7212

Comparing the expressions given in (8) and (9), it can be seen that the mean square ripple produced by *0121* and *7212* are equal at $\alpha = 30^0$ for any value of V_{REF}. However, for $\alpha < 30^0$, *0121* results in smaller ripple than *7212*. For $\alpha > 30^0$, *7212* produces smaller ripple than *0121*. Comparison of 0121 and 7212 in V_{REF}-α plane is shown in Fig. 19.

Comparison of 0127 and 0121

From (5) and (8), the zones of superior performance of *0127* and *0121* can be identified. Sequence *0121* results in smaller ripple in the spatial region above the solid line in Fig. 20, while *0127* results in smaller ripple below the solid line.

Comparison of 0127 and 7212

From (5) and (9), the zones of superior performance of *0127* and *7212* can be identified. Sequence *7212* leads to smaller ripple in the spatial region above the dashed line in Fig. 20, while *0127* results in smaller ripple below the dashed line.

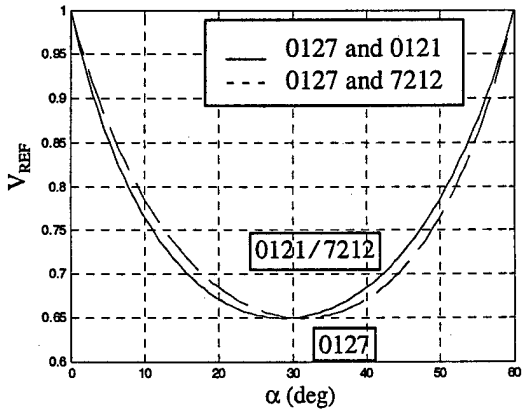

Fig. 20. Comparison of *0121* and *7212* against 0127 (zones of superior performance)

Comparison of 0127, 0121 and 7212

Figs. 19 and 20 together give a comparison of the sequences *0127, 0121* and *7212*. The region above the solid line in the left half of Fig. 20 is the zone of superior performance of *0121*. The region above the dashed line in the right half of Fig. 20 is the zone of superior performance of *7212*. The remaining spatial region is the zone of superior performance of *0127*.

Fig. 21 shows the three-zone hybrid PWM technique I, in the V_{REF}-α plane and in the space vector plane. The zones of superior performance of sequences *0127, 0121* and *7212* are shown in the space vector plane as A, B_1 and B_2, respectively. Sequences *0127* and *7210* are used in alternate sub-cycles in zone A. Sequences *0121* and *1210*, and sequences *7212* and *2127* are used in alternate sub-cycles in zones B_1 and B_2, respectively. As seen from Fig. 21, the two new sequences, *0121* and *7212*, excel for higher values of V_{REF}. From analytical and simulation results, it is seen that the three-zone hybrid PWM technique I reduces THD by 44% at maximum V_{REF}, compared to conventional SVPWM.

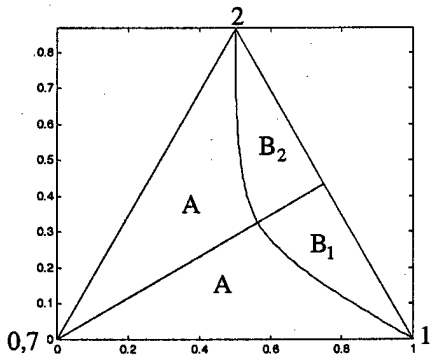

Fig. 21. Three-zone hybrid PWM technique I space vector plane (Sector I)
Zone A : Sequences 0127, 7210, ...
Zone B_1 : Sequences 0121, 1210, ...
Zone B_2 : Sequences 7212, 2127, ...

Figs. 22a and 22b present the measured spectra of line-line voltage for conventional space vector PWM and the proposed three-zone hybrid PWM, respectively, at a fundamental frequency of 60Hz and average switching frequency of 3 kHz. The reduction in the harmonic contents in the three-zone hybrid PWM can be seen clearly.

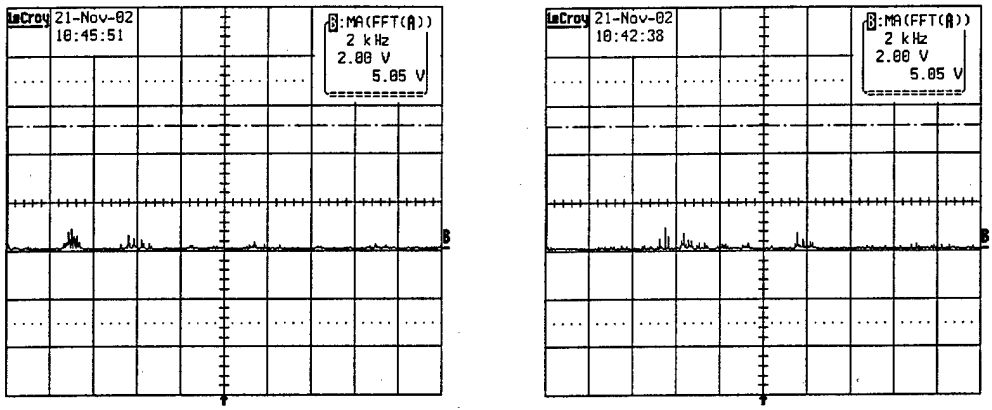

(a) (b)

Fig. 22. Measured spectra of PWM voltage waveform (line-line) at $V_{REF} = 0.866$, $F_1 = 60$Hz, for (a) CSVPWM and (b) three-zone hybrid PWM. Switching frequency is 3kHz for both.

Another interesting characteristic of the hybrid PWM as seen from Fig. 22b, is that the dominant harmonic has shifted to twice the average switching frequency. This is due to the use of the new sequences almost through out the entire sector.

Figs. 23a and 23b present similar spectra at a fundamental frequency of 50Hz and the same switching frequency as above. As seen, the spectrum is more spread out, and the component at the switching frequency is significant. This is due to the use of both conventional and new sequences at lower V_{REF} as indicated in Fig. 21. Figs. 24a to 24d show the no-load current waveforms corresponding to the spectra shown in Figs. 22 and 23. The measured THD in the no-load current are also indicated in each of the figures.

The simulation results showing V_{WTHD} vs. frequency for the conventional PWM

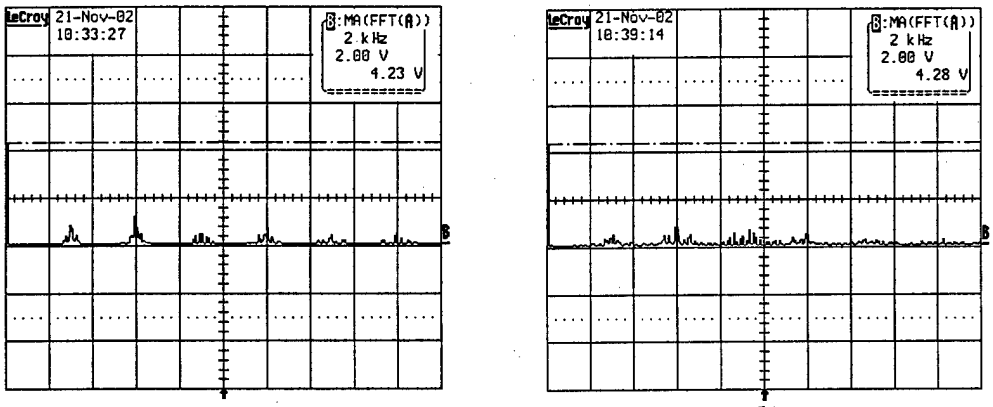

(a) (b)

Fig. 23. Measured spectra of PWM voltage waveform (line-line) at $V_{REF} = 0.722$, $F_1 = 50$Hz, for (a) CSVPWM and (b) three-zone hybrid PWM. Switching frequency is 3kHz for both.

and three zone hybrid PWM I are shown in Fig. 25. The corresponding experimental results, which show I_{THD} vs. frequency, at a switching frequency of 1.5 kHz, are shown in Fig. 26.

It can be easily seen from the plots that the experimental results agree well with the

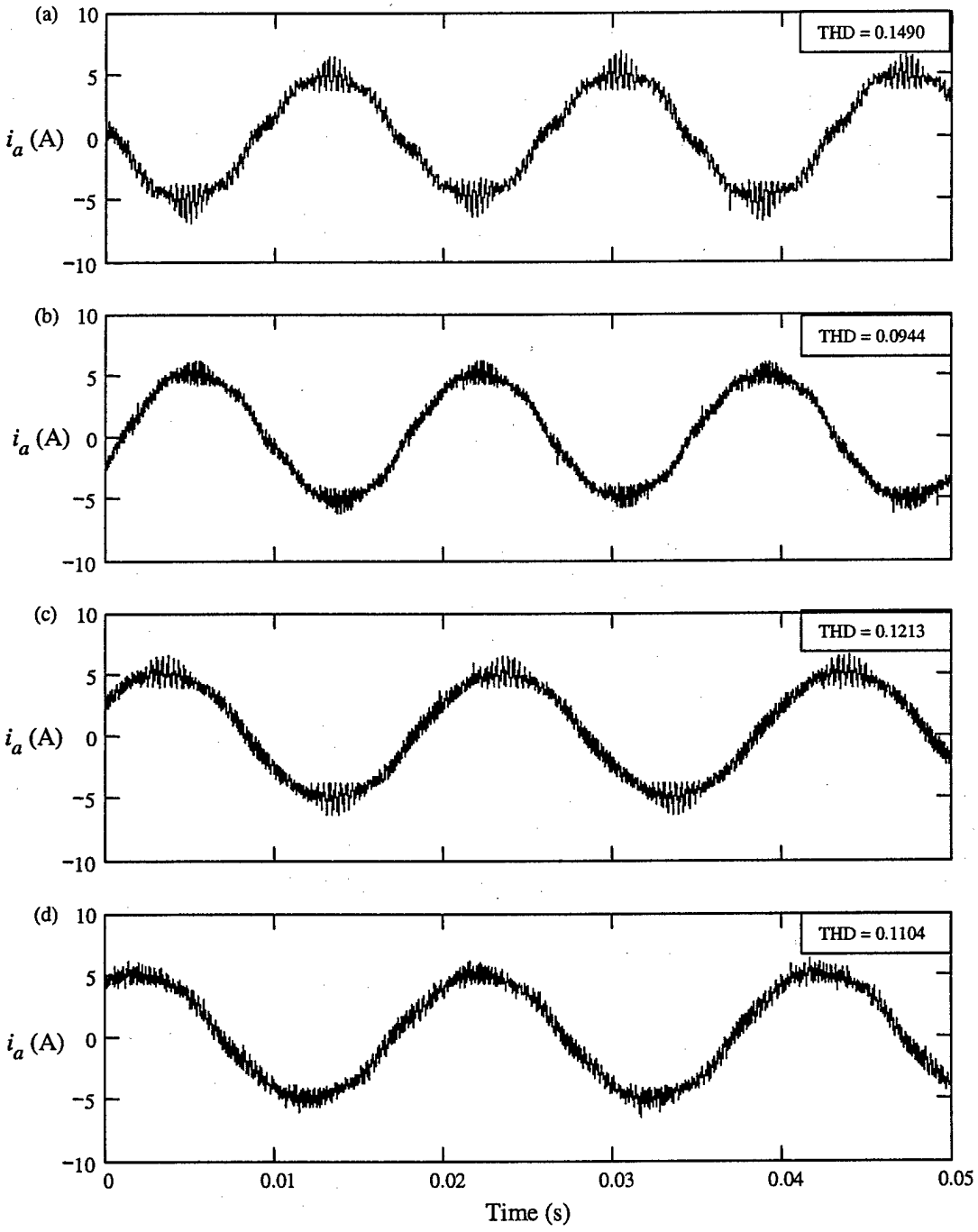

Fig. 24. Measured no-load current (a) CSVPWM at F_1=60Hz, (b) three-zone hybrid PWM I at F_1=60Hz, (c) CSVPWM at F_1=50Hz and (d) three-zone hybrid PWM I at F_1=50Hz

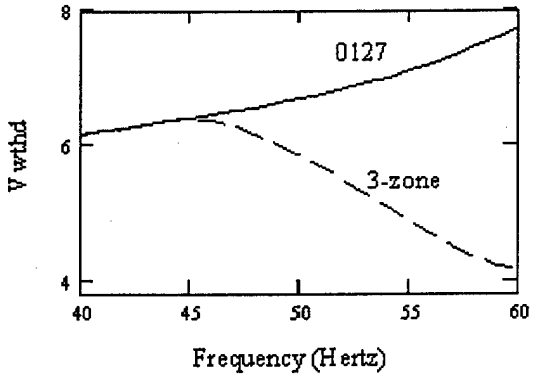

Fig. 25. Analytical results of V_{WTHD} vs. fundamental frequency for conventional SVPWM and 3-Zone hybrid PWM I.

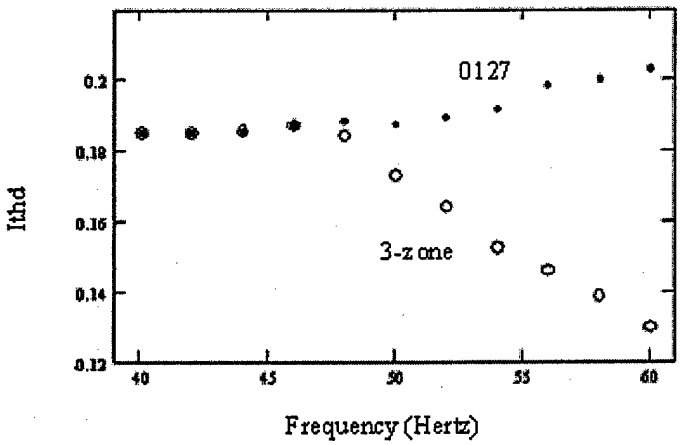

Fig. 26. Experimental results of I_{THD} vs. fundamental frequency for conventional SVPWM and 3-Zone hybrid PWM I.

analysis and that the hybrid technique performs better than the conventional technique at higher modulation indices. The hybrid technique results in an improvement of 44% in comparison to the conventional sequence at the highest modulation index.

4.4 Three-Zone Hybrid PWM Technique II: *0127, 1012* and *2721*

From the analysis of THD in the no-load line current, and from experimental results it was found that the three-zone hybrid PWM technique II, does not result in significant reduction of distortion compared to the conventional space vector PWM. However, the sequences *1012* and *2721* can have significant impact on the switching losses. Hence, the analysis, and expressions for mean square stator flux ripple obtained for these sequences are important for later study, which involves design of hybrid PWM techniques to reduce

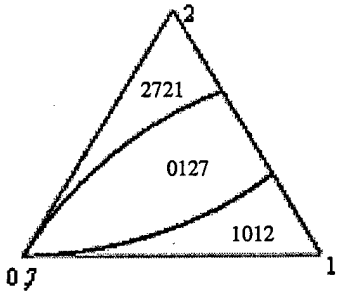

Fig. 27. Three-zone hybrid PWM technique II shown in the space vector plane (Sector I)

both THD as well as switching losses. The division of zones in the space vector plane corresponding to the three-zone hybrid PWM II is shown in Fig. 27.

4.5 Five-Zone Hybrid PWM Technique

The five-zone hybrid PWM technique involves sequences *0127, 0121, 7212, 1012,* and *2721.* As discussed with respect to the three-zone hybrid PWM earlier, the sequences *1012* and *2721* do not result in significant improvement in THD. Hence, the THD performance of the five-zone hybrid PWM is expected to be only marginally better than the three-zone technique – I.

The five-zone PWM technique is shown in Fig. 28 in both the V_{REF}-α plane and in the space vector plane. The simulation results for the five-zone technique are shown in

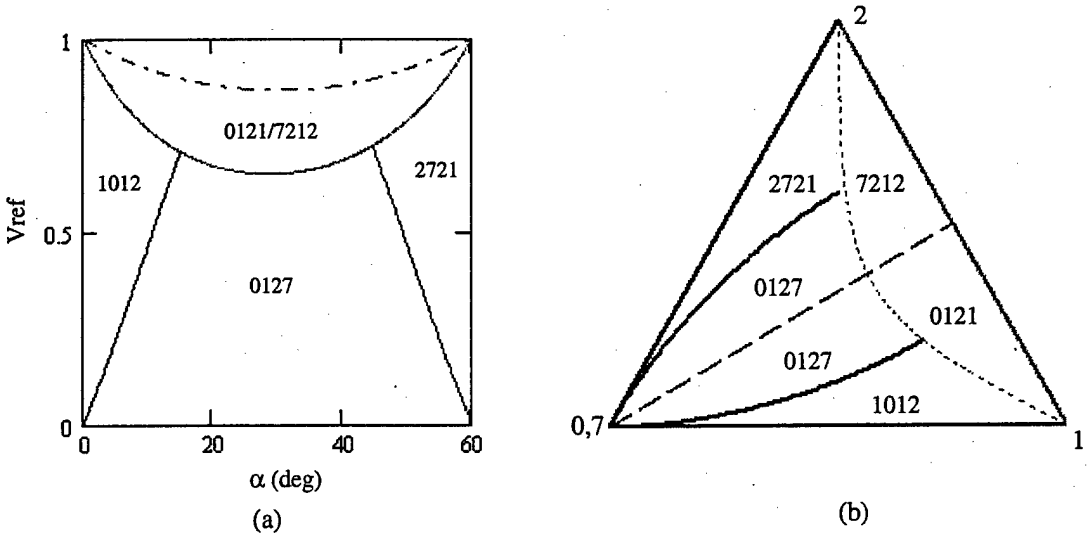

Fig. 28. Five-zone hybrid PWM technique (a) in V_{REF} – α plane and (b) in space vector plane

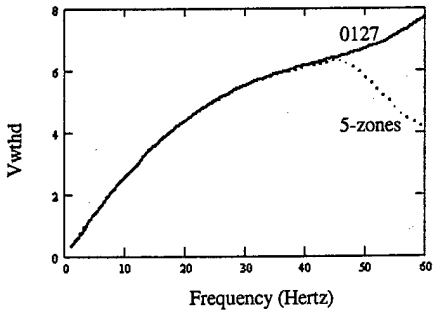

Fig. 29. Analytical results of V_{WTHD} vs. frequency for CSVPWM and Five-Zone hybrid PWM

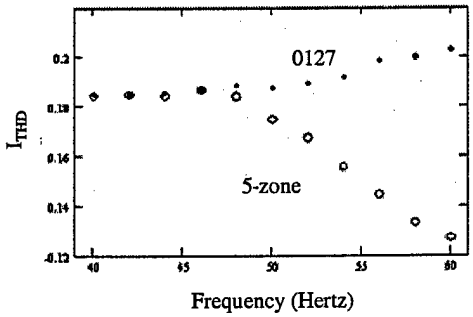

Fig. 30. Experimental results showing I_{THD} vs. frequency for CSVPWM and Five-Zone hybrid PWM

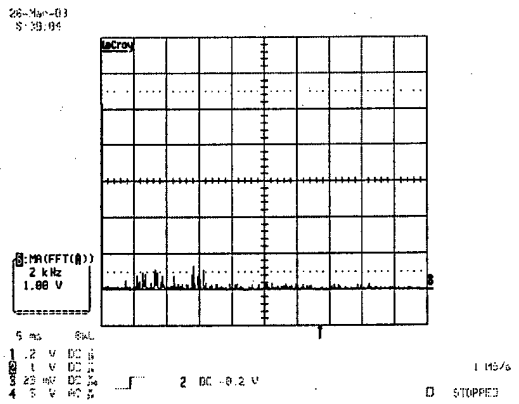

Fig. 31. Measured spectra of PWM voltage waveforms (line-line) corresponding five-Zone hybrid PWM, at a fundamental frequency of 60 Hz

Fig. 29. The corresponding experimental results are shown in Fig. 30. As seen, the five-zone technique results only in a marginal improvement over the three-zone technique I involving sequences *0127, 0121* and *7212.* The new sequences *1012* and *2721* do perform better than the other sequences in some zones, however, the distortion corresponding to these zones are already very small even with conventional sequence. Therefore, *1012* and *2721* do not lead to large savings. The five-zone technique results in

a savings of 46% in THD over the conventional sequence at the maximum modulation index.

The measured spectrum of the PWM voltage waveform (line-line) corresponding to the five-zone PWM, at a fundamental frequency of 60 Hz, is shown in Fig. 31. The experimental no-load line current corresponding to this technique is shown in Fig. 32.

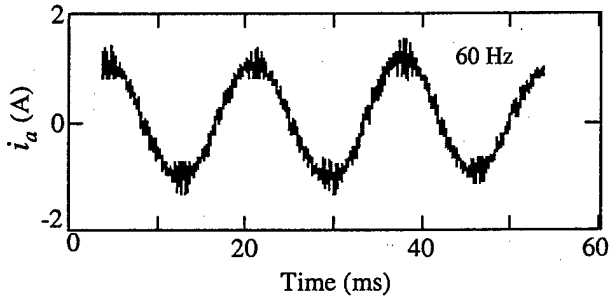

Fig. 32. No-load current waveform corresponding to five-zone hybrid PWM.

4.6 Seven-Zone Hybrid PWM Technique

The seven-zone hybrid PWM involves all the seven possible sequences. It results in savings of 47% in THD compared to the conventional space vector PWM, at a fundamental frequency of 60 Hz that corresponds to maximum V_{REF}. The seven-zone hybrid PWM technique utilizes twin-sampling frequency such that the average switching frequency is the same as the other techniques. Whenever sequences *012* and *721* (which result in only two switchings per sub-cycle) are used, the sampling frequency is made 1.5 times that of other sequences.

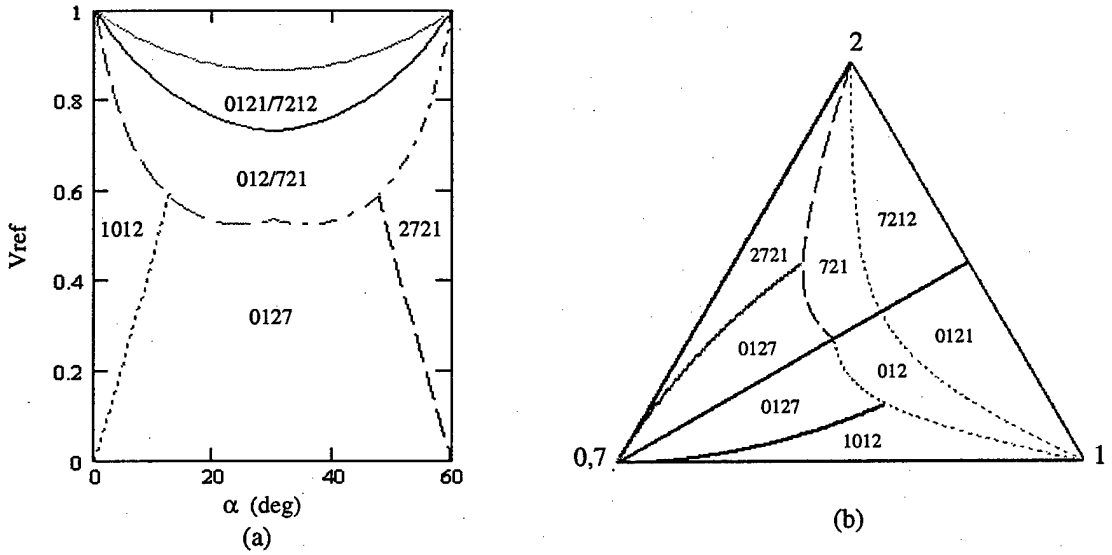

Fig. 33. Seven-zone hybrid PWM technique (a) in V_{REF} – α plane and (b) in space vector plane

The zones of superior performance for each of the seven possible sequences are identified following the procedure described earlier and comparing expressions (5) to (11). Fig. 33 shows the resulting seven-zone hybrid PWM technique in the V_{REF}-α plane and in the space vector plane. The analytical plots of V_{WTHD} vs. frequency corresponding to the seven-zone technique are shown in Fig. 34. The corresponding experimental plots

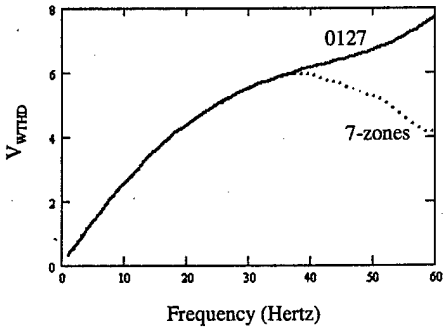

Fig. 34. Analytical results of V_{WTHD} vs. frequency for seven-zone hybrid PWM

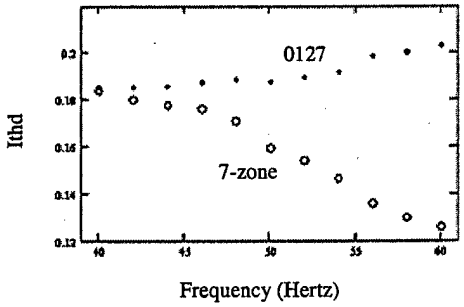

Fig. 35. Experimental results of I_{THD} vs. frequency for seven-zone hybrid PWM

of I_{THD} are shown in Fig. 35. The measured spectrum of the PWM voltage waveform (line-line) is shown in Fig. 36. The measured no-load current waveform, at a fundamental frequency of 60Hz, is shown in Fig. 37.

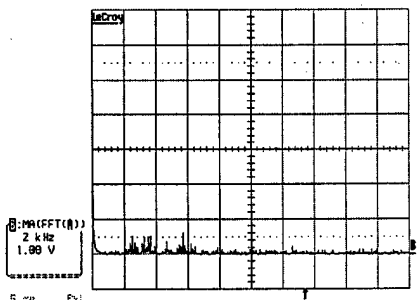

Fig. 36. Measured spectra of PWM voltage waveforms (line-line) corresponding seven-zone hybrid PWM, at a fundamental frequency of 60 Hz

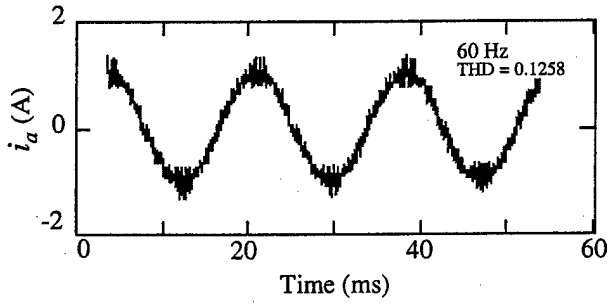

Fig. 37. No-load current waveform corresponding to five-zone hybrid PWM.

The comparison of all the three new hybrid techniques along with the conventional SVPWM in terms of analytical V_{WTHD} is shown in Fig. 38. Comparison of the experimentally obtained I_{THD} vs. frequency plots for all the four techniques are shown in Fig. 39, corresponding to an average switching frequency of 1.5 kHz. The reduction in

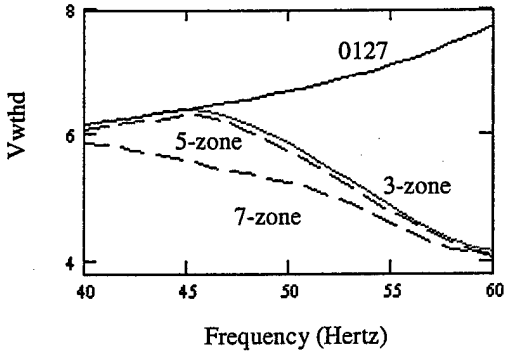

Fig. 38. Comparison of the three THD-based hybrid techniques with CSVPWM in terms of analytical VWTHD vs. frequency

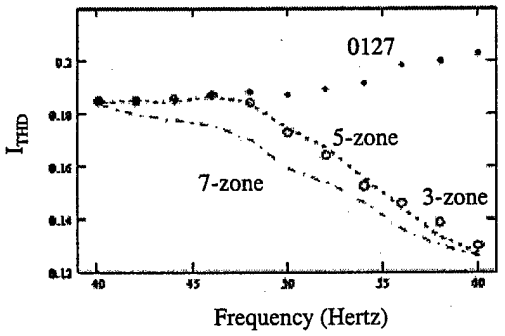

Fig. 39. Comparison of the three THD-based hybrid techniques with CSVPWM in terms of experimental I_{THD} vs. frequency

THD achieved by each of the three new hybrid PWM techniques over the conventional space vector PWM are given in Table II. The reduction is calculated as given in (14).

$$\%\,\text{Reduction} = \frac{I_{THD\_CSVPWM} - I_{THD\_Hybrid}}{I_{THD\_CSVPWM}} \times 100 \quad \ldots \quad (14)$$

TABLE II - REDUCTION IN THD IN HYBRID PWM TECHNIQUES COMPARED TO CSVPWM

PWM Technique	Experimental I_{THD} at 60 Hz	% Reduction over CSVPWM	
		By experiment	By analysis
Conventional	0.2029	0	0
Three-zone I	0.1300	36%	44%
Five-zone	0.1272	37%	46%
Seven-zone	0.1258	38%	47%

5. HYBRID PWM TECHNIQUES TO REDUCE SWITCHING LOSS

Hybrid PWM techniques that use different sequences in different sub-cycles of the same sector, with the objective of reducing THD in the line current, have been developed in the previous section. In this section, the switching loss characteristics of the different sequences are analyzed. Based on this analysis, a new hybrid technique that minimizes the switching losses in the inverter is developed.

5.1 Possibility of Reducing Switching Loss

In a voltage source inverter, the overlap of high currents and high voltages during turn-on and turn-off of the switches result in switching losses. The switching loss in each switching transition depends mainly on the dc bus voltage, instantaneous line current, and turn-on and turn-off transition times. The average power lost is the product of the loss per switching transition and the number of switchings per unit time.

The switching loss per switching transition is independent of the PWM technique applied. Hence, the switching loss characteristics of the different sequences differ only based on the number of switchings in a phase per sub-cycle in relation to the instantaneous magnitude of the corresponding phase current. When the conventional sequence, *0127*, is applied, each phase always switches once in a sub-cycle in all the sectors. When a bus-clamping sequence – *012* or *721* is applied, each phase switches once in four of the six sectors and is clamped during the remaining two sectors. This results in the average switching frequency over a fundamental cycle being less than that of conventional sequence. Hence, for the purpose of comparison in terms of both THD and switching losses, the sampling frequency corresponding to the two bus-clamping sequences is chosen higher than that of other sequences by a factor of 1.5, thus maintaining the average frequency the same for all sequences.

With conventional sequence *0127* and the existing bus clamping sequences *012* and *721*, there cannot be more than one switching per sub-cycle for a given phase. However, as discussed earlier, a distinguishing feature of the new sequences *0121, 7212, 1012* and *2721* that involve active vector division, is that there can be multiple switchings in a given phase per sub-cycle. Specifically, with the new sequences applied, each phase switches once in two of the six sectors, switches twice in another two sectors, and is

clamped in the remaining two sectors. For a given sequence, the sub-cycles in which a particular phase experiences double switching, single switching or clamping is fixed. Total switching loss can be reduced by carefully ensuring that the double switching sequence corresponding to a phase is chosen only when the instantaneous phase current is near its zero crossing, and clamping occurs when the current is near its peak value. Hence, as discussed in detail in subsequent sections, the choice of sequence depends mainly on the power factor of operation, which determines the instantaneous current values in a given sub-cycle.

5.2 Effect of Different Sequences on the Switching Losses

The loss per switching depends on the DC bus voltage, instantaneous line current and the turn-on and turn-off times of the switch. The DC bus voltage remains constant, and the turn-on and turn-off times are also assumed here to be constant for different values of instantaneous line currents. Therefore, switching loss for a given phase in a given sub-cycle depends only on the product of the instantaneous line current and the number of switchings for that phase in the given sub-cycle. Initially, the switching loss characteristic of a sequence is analyzed for the case where the same sequence is applied throughout a sector. In order to compare the switching loss characteristics of sequences over a complete fundamental cycle, it is enough to consider just one phase, since symmetry ensures that the losses in the other phase will also be the same, and the total loss is three times the loss in phase 'a'.

The switching loss factor corresponding to phase 'a' referred to as Ls_a, is defined in (15). It is the product of instantaneous line current in a sub-cycle and the number of switchings in phase 'a' in the given sub-cycle. The integral of the switching loss factor over a complete fundamental period determines the total switching loss in phase 'a'.

$$Ls_{a_k} = \left|i_{ak}\right| \cdot n_{ak} \qquad \ldots \qquad (15)$$

where, i_{a_k} is the magnitude of the instantaneous line current in phase 'a' in the k^{th} sub-cycle and n_{a_k} is the number of switchings in phase 'a' in the k^{th} sub-cycle. Under steady state, the line current of an induction motor is sinusoidal (neglecting high frequency

ripple), and is lagging the line voltage by the power factor angle ϕ. To simplify the analysis, i_{a_k} is normalized, to the peak value of the line current.

Fig. 40 shows the PWM waveforms and the corresponding switching loss factor for phase 'a' at a power factor angle of 30^0 leading, for different types of sequences. For each sequence the average of the switching loss factor over a fundamental period is also shown (dotted lines). Fig. 40a shows the magnitude of the instantaneous line current corresponding to phase 'a'. Fig. 40(b) shows the PWM waveform corresponding to the conventional sequence *0127* and the corresponding switching loss factor. Since, *0127* always has just one switching per sub-cycle, the switching loss factor also has identical waveform as that of the magnitude of the line current.

Fig. 40c shows the PWM waveform and switching loss factor when sequence *0121* is applied throughout sector I. It results in single switching in sectors I and IV, double switching in sectors II and V, and clamping in sectors III and VI. Hence, the switching loss factor is same as the instantaneous current in sectors I and IV, twice the instantaneous current in sectors II and V and zero in sectors III and VI. It can be seen that, with the power factor of 30^0 leading, the peak of current occurs in sectors III and VI, where the phase is clamped and there is no switching. Although the switching loss factor twice the instantaneous current in sectors II and V, because the current magnitude is low in these sectors, the increase in switching loss is less than the reduction achieved in sectors III and VI. Hence, applying sequence *0121* throughout sector I (and sequences corresponding to *0121* in other sectors) results in significant overall reduction of switching losses at the given power factor of 30^0 leading as seen from the average switching loss factor shown in Fig. 40c.

In contrast, Fig. 40d shows the PWM waveform when sequence *2721* is applied throughout sector I (and sequences corresponding to *2721* in other sectors). It is seen that double switching occurs when the instantaneous current is at the peak. Hence, applying *2721* throughout sector I results in increased switching losses, compared to the conventional, at the given power factor of 30^0 leading. Therefore, the average switching loss factor shown in dotted lines is higher than that of conventional sequence.

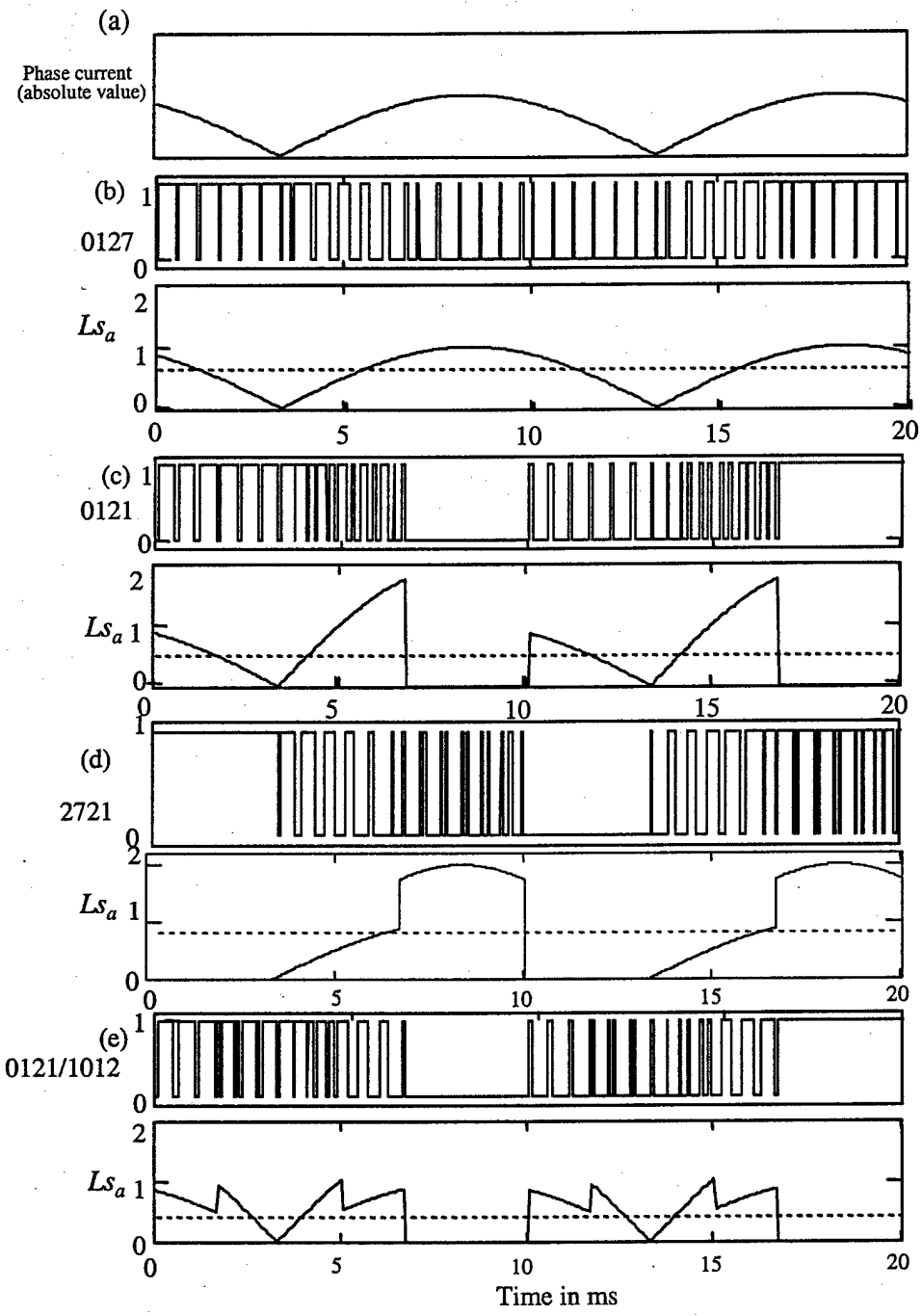

Fig. 40. Switching loss factor over a fundamental period for phase 'a' corresponding to different sequences at power factor angle of 30º. (a) line current magnitude, (b) 0127, (c) 0121, (d) 2721 and (e) 0121/1012

Fig. 40e shows a possible hybrid PWM scheme, where *0121* is used for $0<\alpha<30^0$ and *1012* for $30^0<\alpha<60^0$. As seen, the switching loss factor with such a scheme is significantly reduced as seen from Fig. 40e.

From Fig. 40, it can be concluded that, to reduce switching losses, it is essential to ensure that the double switching occurs when the magnitude of the instantaneous line current is low, and clamping occurs when the instantaneous current magnitude is near its peak value. For a given sequence, the sectors in which single or double switching or clamping occurs is fixed. Therefore, the switching loss factor, and therefore the total switching loss, depends mainly on the load power factor or the angle by which the line current lags or leads the line voltage. Also, it may be noted that the effect of different sequences on the switching loss does not depend on V_{REF} or the fundamental frequency.

Fig. 41 shows the normalized, total switching loss for phase 'a' corresponding to different sequences as a function of power factor angle. The normalized, total switching loss is just the integral of the switching loss factor over a fundamental period normalized to the switching loss corresponding to the conventional sequence. Note that, in this analysis the same sequence is applied throughout the sector. As seen, different sequences perform better at different power factor angles. At the power factor of 30^0 leading, sequence *1012* results in 25% reduction in switching losses, and sequence *2721* results in 25% increase in switching losses, both of which can be explained by the waveforms shown in Fig. 40.

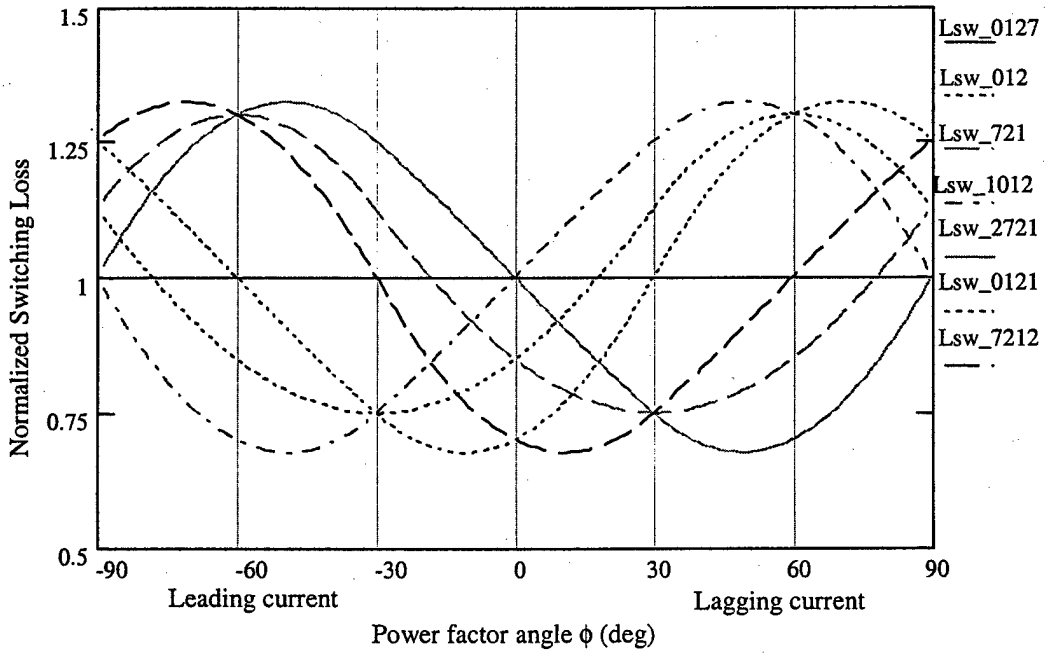

Fig. 41. Total switching loss of different switching sequences (applied over the entire sector) normalized to that of CSVPWM

5.3 Switching Loss Optimized Hybrid PWM Technique

From Fig. 41, it can seen that there is no single sequence that results in the lowest switching loss throughout the whole range of power factor from 90^0 leading to 90^0 lagging. Hence, hybrid PWM techniques, which use a combination of different sequences, each applied at the appropriate sub-cycles, are required. Since, switching loss is independent of fundamental frequency or V_{REF}, in order to design hybrid PWM techniques aimed at reducing switching loss, the $\alpha-\phi$ plane (instead of the α-V_{REF} plane as in THD study) needs to be partitioned into zones of superior performance for different sequences.

The seven sequences need to be compared against each other on a sub-cycle basis to determine the regions of superior performance. Therefore, at each point in the $\alpha-\phi$ plane, the *three-phase switching loss factor*, $Ls_{3\phi}$, as defined in (16), for each of the seven sequences is calculated and compared. Note that unlike in the previous section, where the same sequence was applied throughout a sector, for a comparison at the sub-cycle level, the sum of switching losses due to all the three phases needs to be considered.

$$Ls_{3\phi_k} = n_{a_k}\left|i_{a_k}\right| + n_{b_k}\left|i_{b_k}\right| + n_{c_k}\left|i_{c_k}\right| \qquad \ldots$$

(16) where, n_{a_k} is the number of switchings in phase 'a' at the k^{th} sub-cycle and i_{a_k} is the instantaneous line current corresponding to phase 'a'. The number of switchings in each phase for different sequences has been listed in Table I in Section 2.2.

The $\alpha-\phi$ plane is divided into zones of superior performance for different sequences, leading to the switching loss optimized hybrid PWM shown in Fig. 42 for the entire range of power factor angles from 90^0 leading to 90^0 lagging. It may be noted that the whenever sequences *012* or *712* are considered, the switching frequency is made 1.5 times as that of the other sequences, in order to maintain the same average switching frequency. It is interesting to note from Fig. 42 that only four of the seven sequences - *1012, 0121, 7212, and 2721*, are used in the hybrid PWM technique for switching loss reduction, and all of these are the new sequences involving division of active state duration. It may be noted that the switching scheme suggested in Fig. 40e is an example of the proposed hybrid PWM technique at the given power factor angle of 30^0 leading.

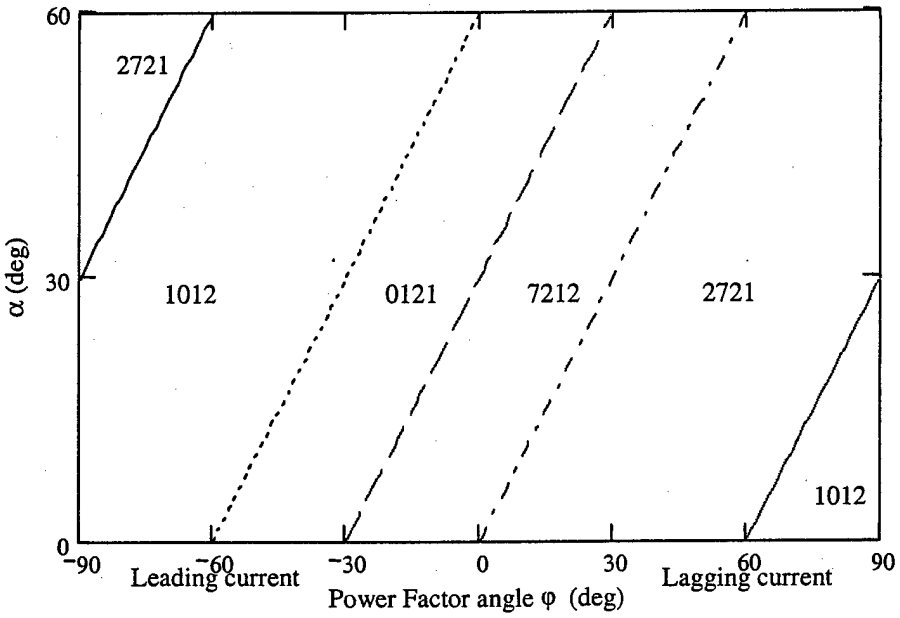

Fig. 42. Switching loss optimized hybrid PWM in the α–ϕ plane

Fig. 43 shows the simulation result comparing the total switching loss of switching-loss-optimized technique with that of conventional SVPWM technique. The switching-loss-optimized technique results in more than 30% reduction in switching loss compared to conventional SVPWM technique over a wide range of power factor angles.

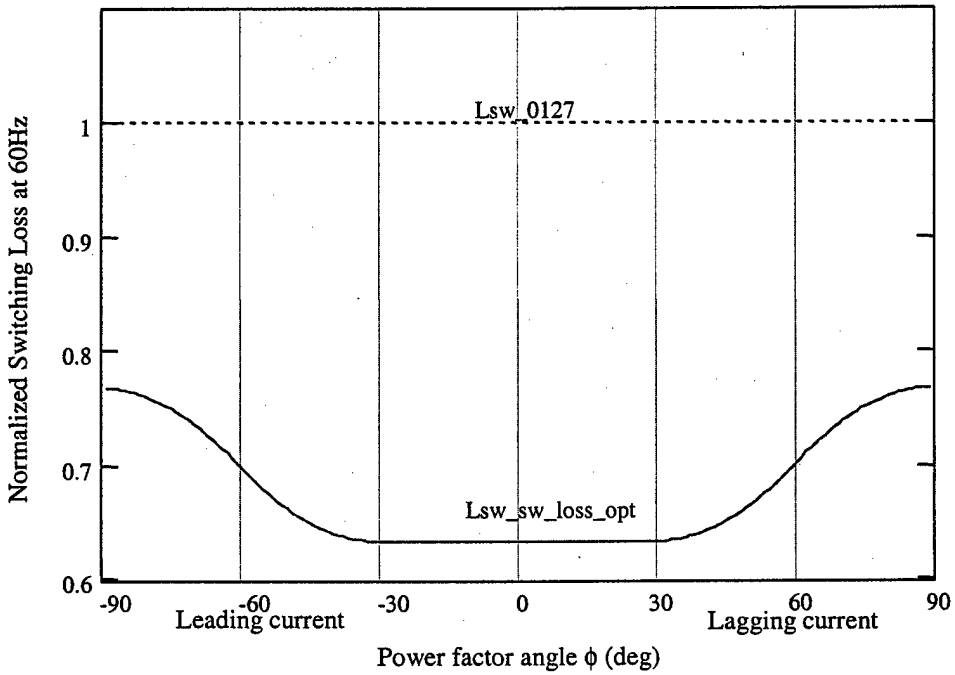

Fig. 43. Comparison of switching loss in CSVPWM and switching-loss-optimized hybrid PWM at different power factor angles, obtained from simulation.

5.4 Experimental Results

The switching-loss-optimized hybrid PWM technique is implemented in the experimental prototype using TMS320F243, a DSP from Texas Instruments with a CPU clock frequency of 20 MHz.

Fig. 44 shows the experimental results comparing the switching-loss-optimized technique and conventional technique. Fig. 44a corresponds to conventional SVPWM and has single switching throughout the fundamental period. Fig. 44b corresponds to the switching-loss-optimized PWM technique at a power factor angle of 30^0 lagging. The double switching occurs near the zero crossing of the line current, and the clamping duration is exactly centered around the peak. This results in significant savings in the switching losses. Fig. 44c corresponds to a power factor angle of 60^0 lagging. As seen, the double switching occurs near the zero crossing of the current, but, the clamping is not centered around the peak of the line current, and hence there is not a significant reduction in the switching loss, just as expected from Fig. 43.

Direct measurement of switching losses by measuring the instantaneous switch current and switch voltage is not practical. Finite differences in the delay times of voltage probes and current probes introduce a large error in power loss measurements, especially considering that the total switching losses, and therefore the savings achieved by the proposed schemes are small. Besides, with an integrated three-phase IGBT module, the terminals are also not easily accessible for current measurements. An alternate approach used here is to compare the temperature rise of the heatsink on which the IGBT is mounted, for different PWM techniques. The temperature rise depends on the total power loss in all the three phases, and includes both conduction losses as well as switching losses. The conduction losses are independent of the PWM technique used. In order to obtain the conduction losses and switching losses separately, the system is operated at two different switching frequencies keeping all other parameters such as dc bus voltage, fundamental frequency and load unchanged. For example, when the switching frequency is doubled, the conduction losses remain the same, and the switching losses are doubled. Therefore, the difference in temperature rise between the two cases corresponds to the temperature rise due to switching losses alone, at the original

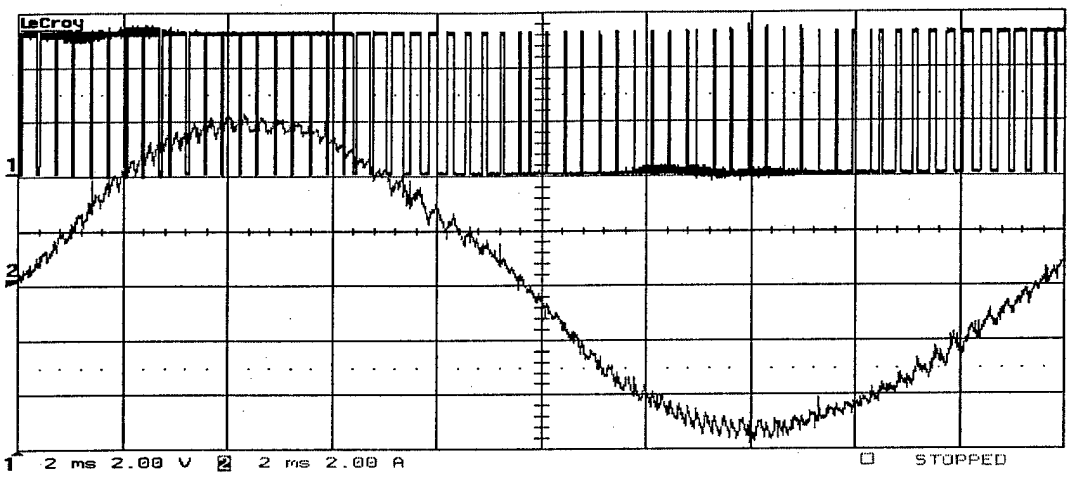

(a) Conventional SVPWM

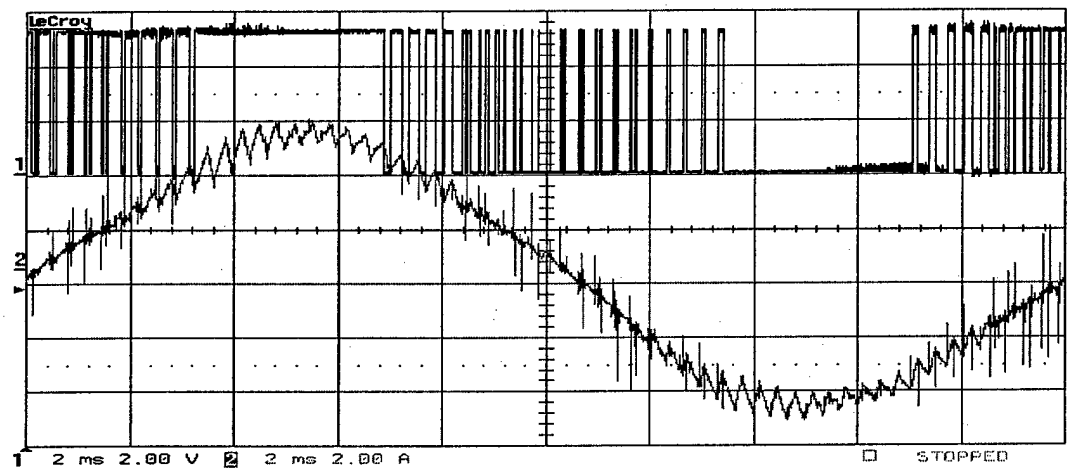

(b) Switching-loss-optimized hybrid PWM corresponding to $\phi = 30^0$ lagging

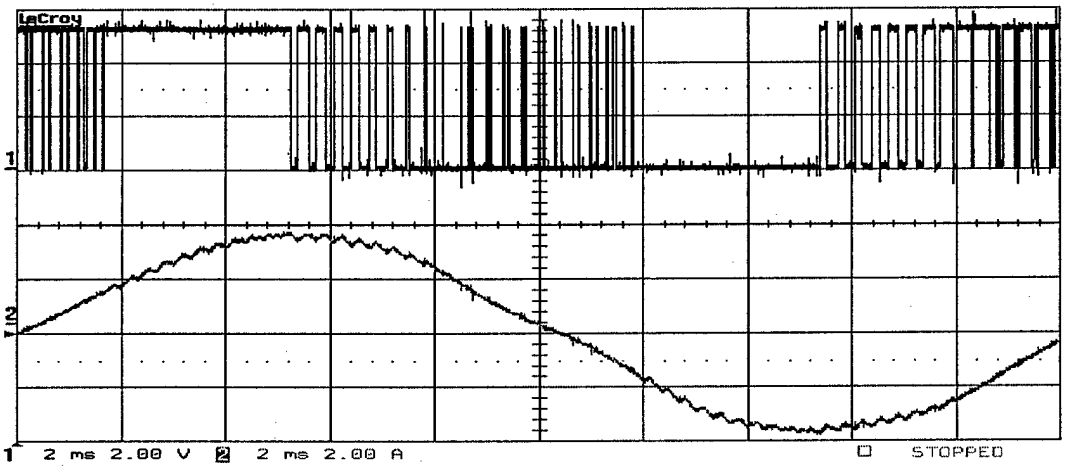

(c) Switching-loss-optimized hybrid PWM corresponding to $\phi = 60^0$ lagging

Fig. 44. Experimental PWM waveforms and line currents of CSVPWM and switching-loss-optimized hybrid PWM at different power factor angles. (Scale: 2A/div and 2ms/div).

switching frequency. The temperature rise due to switching losses alone for the conventional SVPWM, corresponding to the waveforms shown in Fig. 44a is 2.6^0C

where as the temperature rise due to switching losses using the switching-loss-optimized PWM, corresponding to the waveforms shown in Fig. 44c is 2.0^0C. Therefore, the new hybrid PWM technique reduces the switching losses by approximately 30% compared to the conventional SVPWM, which agrees well with simulation results.

6. HYBRID PWM TECHNIQUES FOR SIMULTANEOUS REDUCTION IN THD AND SWITCHING LOSS

In the previous sections hybrid PWM techniques to reduce either the THD in the line current or the switching losses in the inverter have been developed and experimentally validated. The hybrid techniques for THD reduction involved division of the V_{ref} *vs* α plane into zones of superior THD performance, and the hybrid techniques for switching loss reduction involved the division of ϕ *vs* α into zones of superior switching loss performance. In this section, based on the previous analysis of THD and switching loss characteristics of different sequences, hybrid PWM techniques that simultaneously reduce both THD as well as the switching losses are developed.

Fig. 45 compares the performance of the THD-optimized (seven-zone) technique and the switching-loss-optimized technique along with the conventional space vector

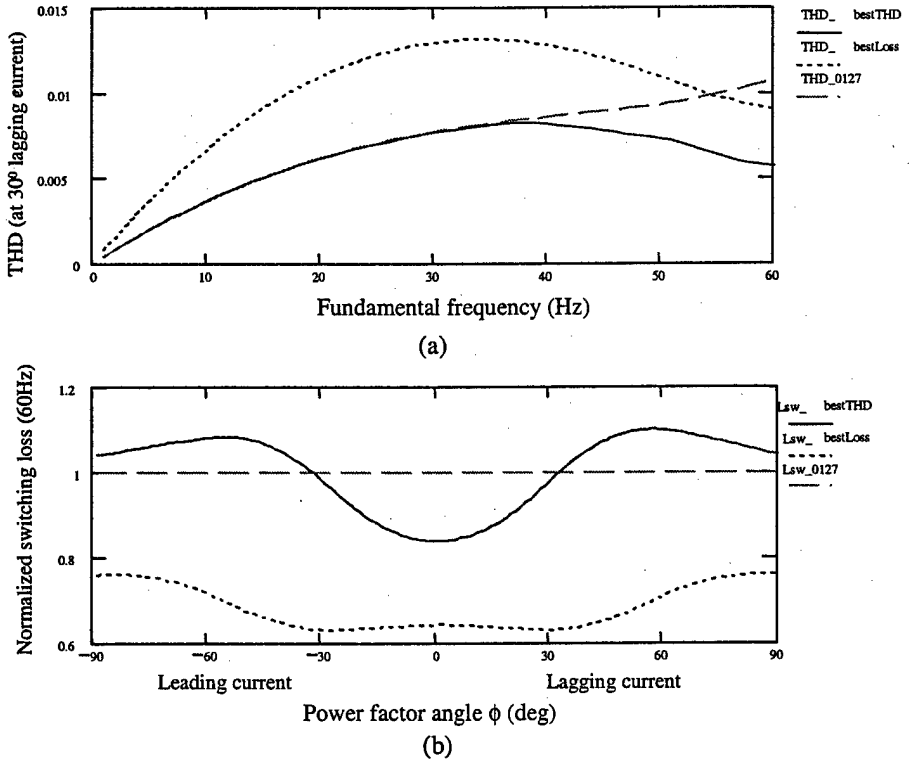

Fig. 45. Comparison of conventional SVPWM, THD-optimized-PWM (seven-zone) and switching-loss-optimized-PWM in terms of THD and switching loss.
(a) THD vs. fundamental frequency (or Vref) at 30^0 lagging power factor angle and
(b) Switching loss vs. power factor angle at 60 Hz

PWM. Fig. 45a shows the THD as a function of the fundamental frequency, and Fig. 45b shows the normalized switching loss as a function of power factor angle, for the above three techniques. It can be seen from Fig. 45 that none of the three techniques result in optimized performance if ***both*** THD and switching losses are to be minimized.

6.1 Hybrid PWM Technique Based on Quality Factor

To develop a new hybrid PWM technique that reduces both THD and switching loss, the goal is still to obtain the zone division of the space vector plane and applying the right sequence in each zone. To evaluate the performance of different sequences on both the switching losses and THD, a new performance index, Q is defined as:

$$Q = W_{THD} \cdot \frac{F_{sequence}}{F_{0127}} + W_{Loss} \cdot \frac{Ls_{3\phi sequence}}{Ls_{3\phi 0127}} \quad \ldots \quad (17)$$

where, F is the mean square ripple for the valid sequences in a given sub-cycle as defined in Section 3, and $Ls_{3\phi}$ is the three-phase switching loss factor of a sequence over a sub-cycle as defined in (16). W_{THD} and W_{Loss} are user-defined weights assigned to THD and switching loss performance, based on the requirements of the given application.

$$W_{THD} + W_{Loss} = 1 \quad \ldots \quad (18)$$

As discussed in Section 3, mean square ripple, F, is a function in the V_{ref} *vs* α plane, and as discussed in Section 5, the switching loss factor is a function in the ϕ *vs* α plane. Therefore, the performance index, Q of different sequences then must be analyzed in a three-dimensional space – V_{REF}, ϕ and α, where V_{REF} is from 0 to 0.866(corresponding to fundamental frequency from 0 to 60 Hz), α is from 0 to 60^0(due to the symmetry, only sector I needs to be considered), and ϕ is from 90^0 leading to 90^0 lagging. The quality factor as defined in (17) corresponding to each valid sequence is calculated and compared at every point in the three-dimensional plane. The sequence that minimizes Q in a given sub-cycle is selected to obtain the desired zone division. It may be noted that, as before, whenever sequences *012* and *721* are considered, the switching frequency is made 1.5 times that of other sequences, in order to maintain the same average switching frequency. Because the zone division is in a three-dimensional space,

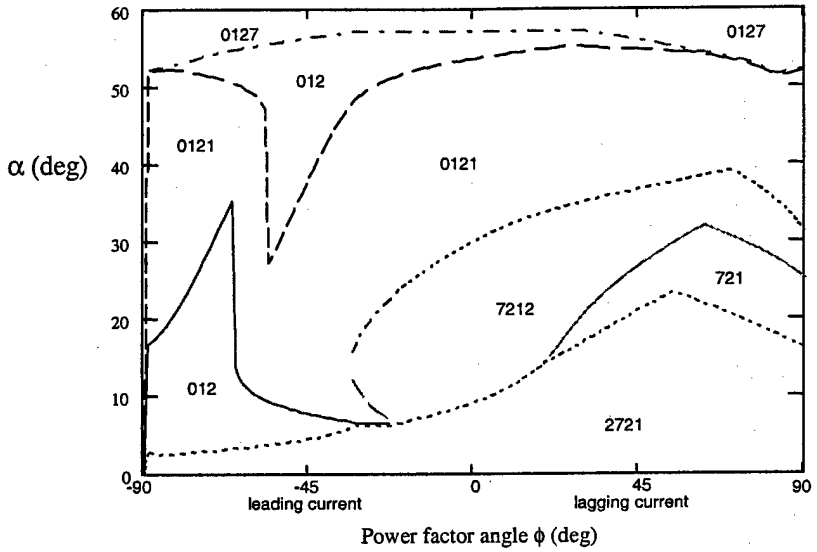

Fig. 46. Zones of superior performance in terms of quality factor at a fundamental frequency of 60Hz

which is too complex to be shown in one plot, only the division corresponding to the nominal fundamental frequency (60 Hz) is shown here in Fig. 46.

Fig. 47 shows the simulation result comparing Q of the new hybrid technique suggested in Fig. 46 and Q of conventional SVPWM technique. The new technique results in 10% to 40% reduction in Q compared to conventional SVPWM technique over a wide range of power factor angle at the considered fundamental frequency of 60 Hz. Though the results shown in Fig. 47 are encouraging, this hybrid PWM technique involving a three-dimensional plane, is too complex to implement using simple digital signal processors, and hence is not very practical.

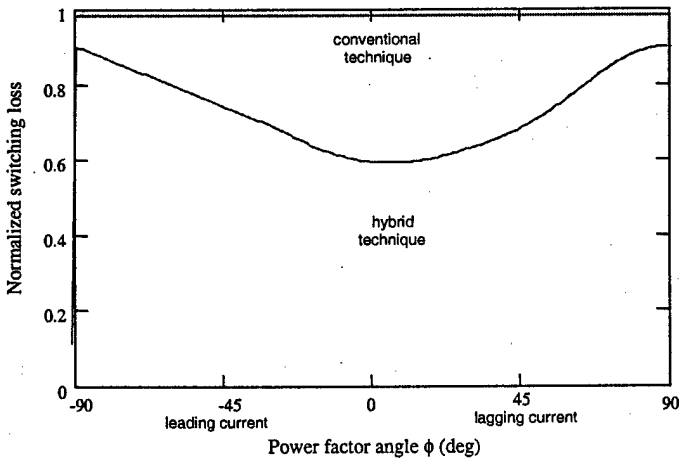

Fig. 47. Simulation results comparing the quality factor for CSVPWM with the hybrid PWM suggested in Fig. 46

6.2. Practical Hybrid PWM Techniques for Reduction of THD and Switching Loss

A more practical approach is to carefully study the THD characteristics and the switching loss characteristics of the different sequences, described in details in Sections 3, 4 and 5, and identify zones of superior performance in the V_{REF}-α plane for a limited range of power factor angles that are typical of the application considered. In this project, a simple PWM technique that reduces both THD and switching losses for induction motor drive applications, where the typical power factor angles range from 20^0 to 60^0, has been developed.

From the hybrid PWM technique for best switching loss performance shown in Fig. 42, it can be seen that for the range of power factor between 20^0 to 60^0 lagging, *7212* is one of the sequences that result in minimum switching losses. Also, from Fig. 41, it can be seen that sequence *0121* results in higher switching loss than conventional sequence for $\phi > 30^0$. The three-zone technique shown in Fig. 21, based on THD considerations, suggests use of *0121* for $0^0 < \alpha < 30^0$ and *7212* for $30^0 < \alpha < 60^0$ and higher values of V_{REF}. However, the difference between the stator flux ripples of *0121* and *7212* is not significant at high values of V_{REF}. But, the sequence *7212* results in significantly lower switching loss than *0121* for typical power factor angles considered. From these observations, a possible PWM technique that simultaneously lowers THD as well as switching loss can be designed and is shown in Fig. 48a as Type I hybrid PWM. The boundary between the zones corresponding to sequence *0127* and sequence *7212* is the same as the boundary separating the superior performance regions of *0127* and *7212* in the THD based three-zone hybrid technique shown in Fig. 21.

Similarly, from Fig. 42 and Fig. 33, which shows the seven-zone PWM technique for THD improvement, some other useful facts can be derived. For the range of power factor between 20^0 to 60^0 lagging, *721* can also result in low switching losses, although not as low as *7212*. However, *721* performs significantly better from THD consideration at lower values of V_{REF}. The seven-zone technique shown in Fig. 32 suggests use of *012* for $0^0 < \alpha < 30^0$ and *721* for $30^0 < \alpha < 60^0$ at low values of V_{REF}. Similar to *0121* and *7212*, the difference between the stator flux ripples of *012* and *721* is not very significant; hence *721* can be used instead of *012* achieving reduction in switching loss without much

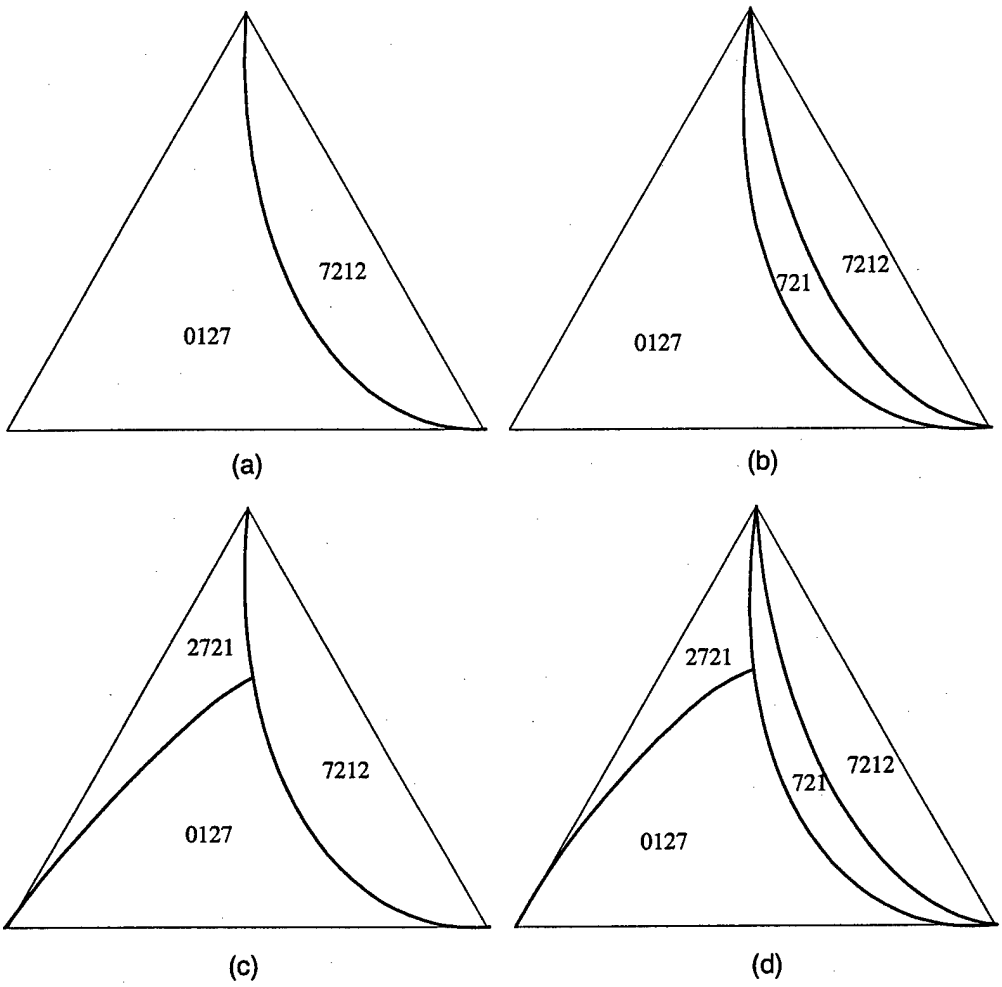

Fig. 48. Four different hybrid PWM techniques to reduce both THD and switching loss
(a) Type I - *0127 and 7212* (b) Type II *0127, 7212 and 721*
(c) Type III *0127, 7212 and 2721* (d) Type IV *0127, 7212, 721 and 2721*

increase in THD. Sequence *2721* is another choice for reducing switching losses at typical power factor angles encountered motor drive applications, as seen in Fig. 42. Also, it can be seen from expressions of stator flux ripple that *2721* results in lower THD when α is close to 60^0. From all these observations, another three possible PWM techniques that simultaneously lower THD as well as switching loss can be obtained as shown in Figs. 48b to 48d.

Simulation results corresponding to THD vs. fundamental frequency (or V_{REF}), obtained with each of the new hybrid PWM techniques shown in Fig. 48, along with that of the conventional SVPWM are shown in Fig. 49a. These plots correspond to a nominal power factor angle of 30^0. It can be seen that introduction of sequence *721*

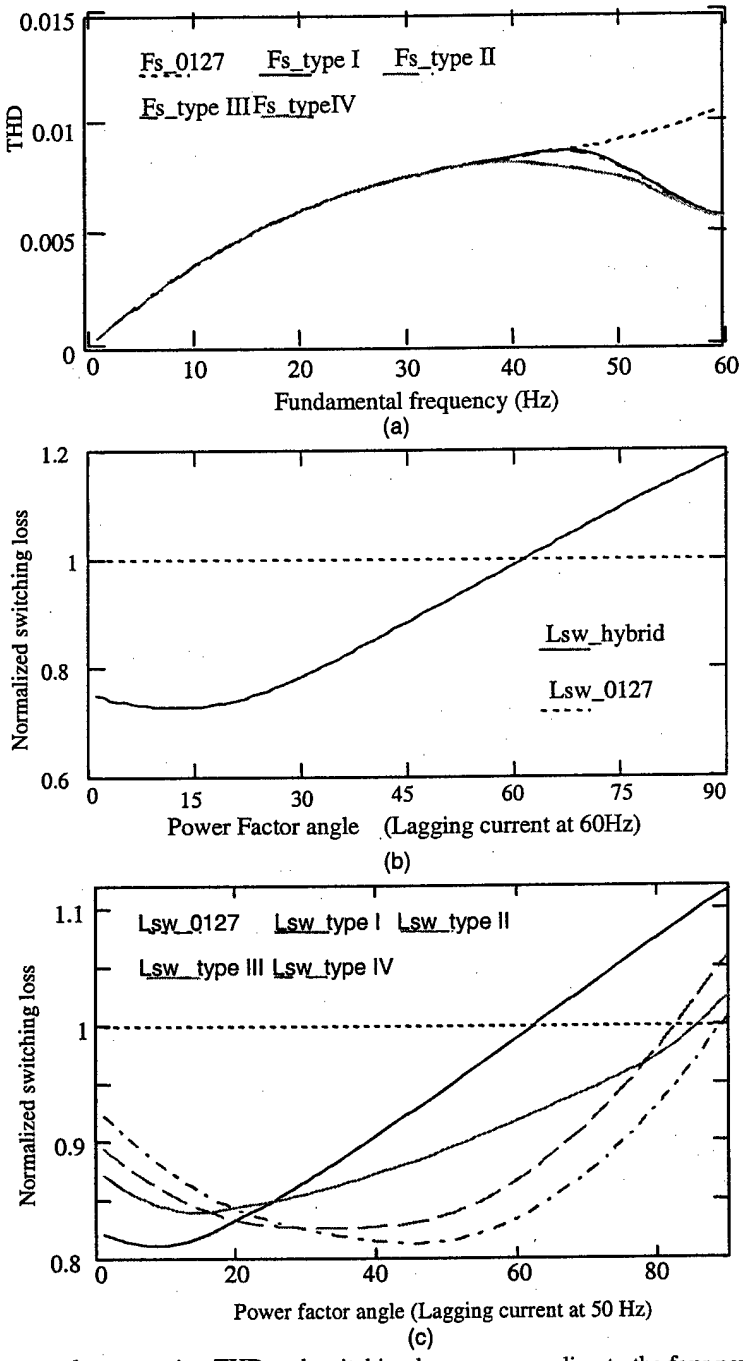

Fig. 49. Simulation results comparing THD and switching loss corresponding to the four new combined hybrid PWM techniques with those of CSVPWM. (a) THD, (b) switching loss at 60 Hz (c) switching loss at 50 Hz

results in significant improvement in THD performance in the fundamental frequency region from 40 Hz to 50 Hz (PWM techniques Type II and Type IV). These new PWM techniques result in more than 30% reduction in THD (in addition to the reduction in switching loss).

Simulation results corresponding to the switching losses produced by each of the hybrid PWM techniques normalized to that of the conventional SVPWM, at 60 Hz, are shown in Fig. 49b. From Fig. 48 it can be seen that at higher fundamental frequency,

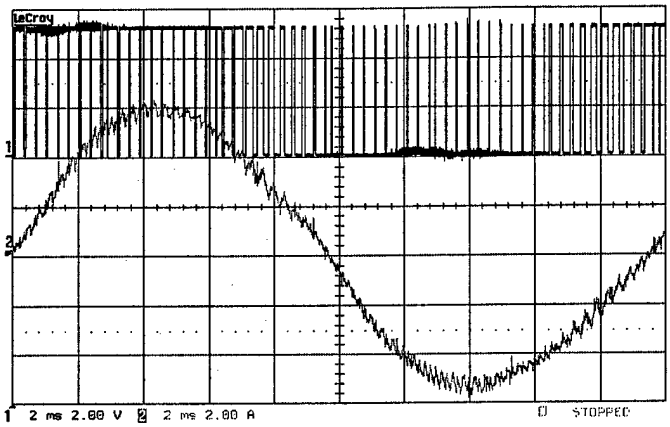

(a) conventional sequence *0127*

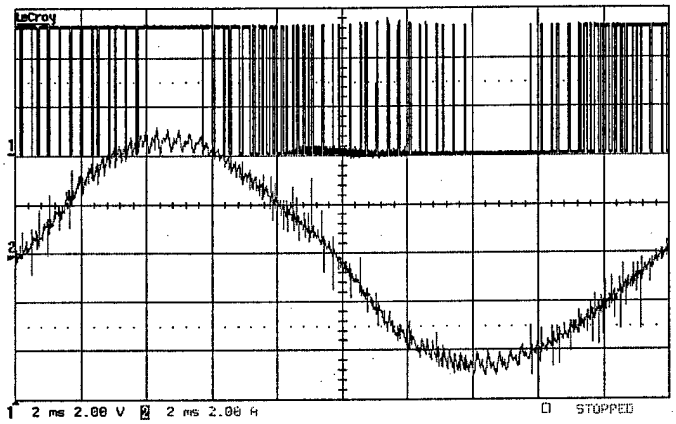

(b) Hybrid PWM technique Type I indicated by Fig. 48a

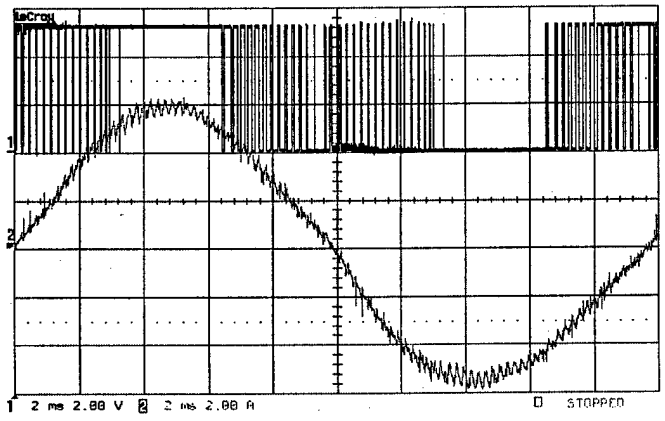

(c) Hybrid PWM technique Type IV indicated by Fig. 48d

Fig. 50. Experimental PWM waveforms and line currents corresponding to CSVPWM and Type I and Type IV hybrid PWM techniques at 50 Hz and at a power factor angle of 30^0 lagging

close to 60 Hz, *7212* is the only mainly used sequence for all the four types of hybrid PWM techniques. Therefore, the curves of the switching loss factors of the four techniques are identical at 60 Hz, but at a lower fundamental frequency, for example, at 50 Hz, the advantages of introducing the sequences *721* and *2721* become obvious. Fig. 49c shows the switching loss curves corresponding to 50Hz. As seen, Type IV PWM results in more than 16% reduction in switching loss throughout the power factor angle range of interest, namely 20^0 lagging to 60^0 lagging. Type IV PWM also achieves the maximum reduction in THD.

The proposed hybrid PWM techniques are easy to implement using standard DSP such as TMS320F243 from Texas Instruments. Fig. 50 shows the PWM waveforms and the line currents corresponding to the hybrid PWM techniques - Type I and Type IV along with those of the conventional SVPWM. All the waveforms correspond to a power factor angle of 30^0 lagging. As seen, PWM using *2721, 7212,* and *721* (Type IV) results in clamping or single switching of phase 'a' around the peak of the current and double switching near the zero crossing of the current. Hence, it results in lower switching loss over a fundamental cycle compared to the conventional sequence. The FFT analysis of the phase current waveforms corresponding to type IV PWM shows a 17% reduction in THD at the fundamental frequency of 50Hz. Higher reduction in THD is possible at higher V_{REF} corresponding to a fundamental frequency of 60 Hz as seen from Fig. 49a.

6.3 Hybrid PWM Techniques with Current Feedback

As discussed in Section 3, the distortion due to different sequences or PWM techniques in a given sub-cycle depend only on V_{REF} and α, which are parameters generated by the controller. However, the switching loss corresponding to the sequences depend on the power factor angle of the motor, which depends on the load and other operating conditions. All the hybrid PWM techniques, to reduce both THD and switching loss, developed in 6.2, have been designed for an assumed range of power factor angles, typically of motor drive applications. Specifically, these techniques do not use actual power factor information. Therefore, the zone division remains identical even when the power factor angle changes. For example, it can be seen from Fig. 49 that the switching loss performance of Type I hybrid PWM becomes worse than even the conventional

SVPWM when the power factor angle goes beyond 60^0 lagging. This is Type I technique continues to use 7212 in most of sector I (corresponding to high V_{REF}), which, as shown in Fig. 41, results in higher switching loss than 0127 for $\phi>60^0$. Also, the switching loss performance of different PWM techniques are very different when $\phi<20^0$. Hence, it can be concluded that by utilizing feedback of motor current and designing new PWM techniques based on the current or power factor angle- information can lead to further reduction in switching loss.

Current peak detection feedback technique

From previous analysis, the basic method of reducing switching loss is to avoid double switching at peak current. Using current feedback, a new hybrid PWM technique is developed based on the five-zone hybrid PWM (THD) described in Fig. 48. In the new technique, Sector I is also divided into zones of superior performance based on THD considerations alone. In addition, for each zone the second best sequence based on THD is also identified. In each sub-cycle, the best sequence that results in minimum THD is applied when it does not cause double switching near current peak. If it involves double switching near current peak, the sequence that results in second best THD performance is applied. Since, the best sequence involves double switching, automatically the second

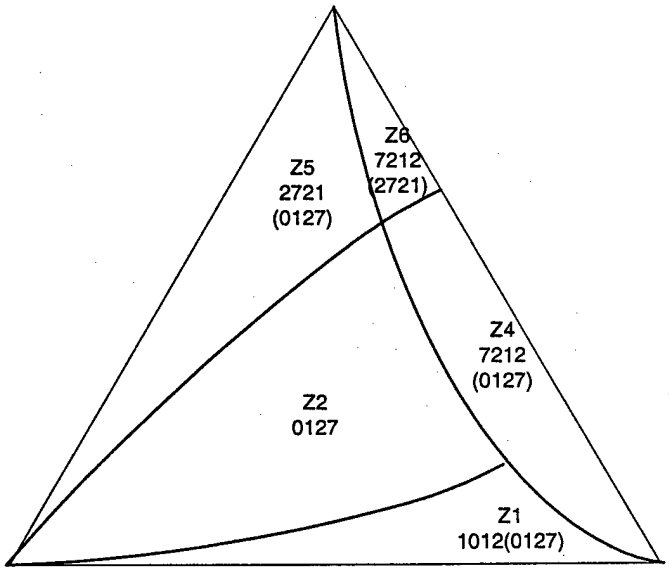

Fig. 51. Hybrid PWM technique utilizing instantaneous current feedback
(sequences in parenthesis correspond to second best THD sequences)

best sequence will not result in double switching. The new hybrid PWM technique with instantaneous current feedback is shown in Fig. 51.

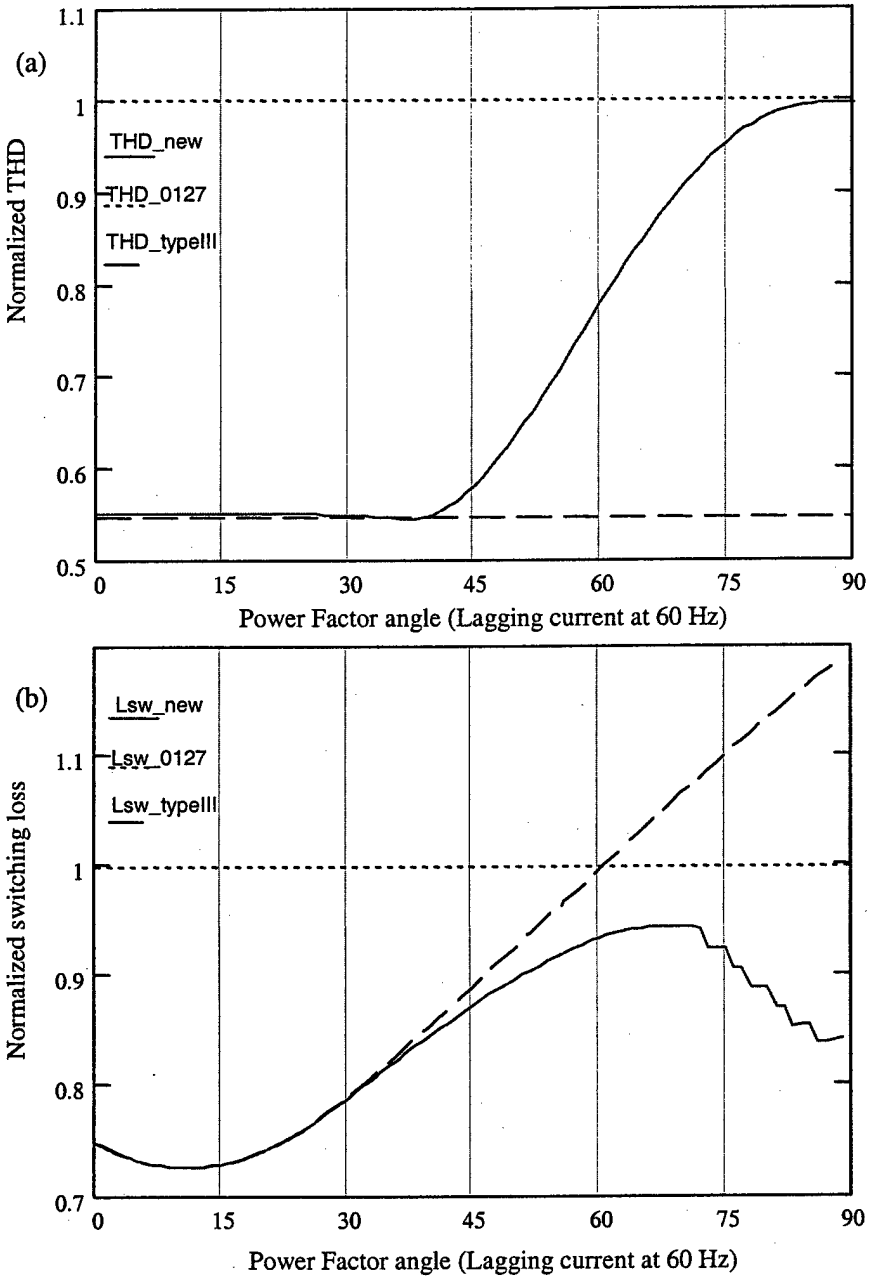

Fig. 52. Simulation results comparing CSVPWM with hybrid PWM technique shown in Fig. 51 (a) THD and (b) Switching loss

The THD and switching loss performance as a function of power factor angle (corresponding to a fundamental frequency of 60 Hz), obtained using the new PWM

technique, along with those of the conventional SVPWM as well as the Type III technique (Fig. 48) are shown in Fig. 52. As seen, the proposed PWM technique improves the switching loss performance when the power factor is near 60^0 lagging, but at the cost of THD performance.

Current peak and power factor angle feedback technique

From Fig. 42, it can be seen that in switching-loss-optimized PWM technique, the boundaries of different zones are functions of the power factor angle of the motor. Hence, utilizing information on power factor angle can possibly lead to an improved PWM technique. A new hybrid PWM technique is proposed in this section that uses power factor angle information also in the zone division (based initially on THD performance) and also used instantaneous current feedback to ensure double switching does not occur near current peak. The zone division for the new PWM technique is shown in Fig. 53 and the zone definitions are given in Table III, where ϕ is the measured power factor angle.

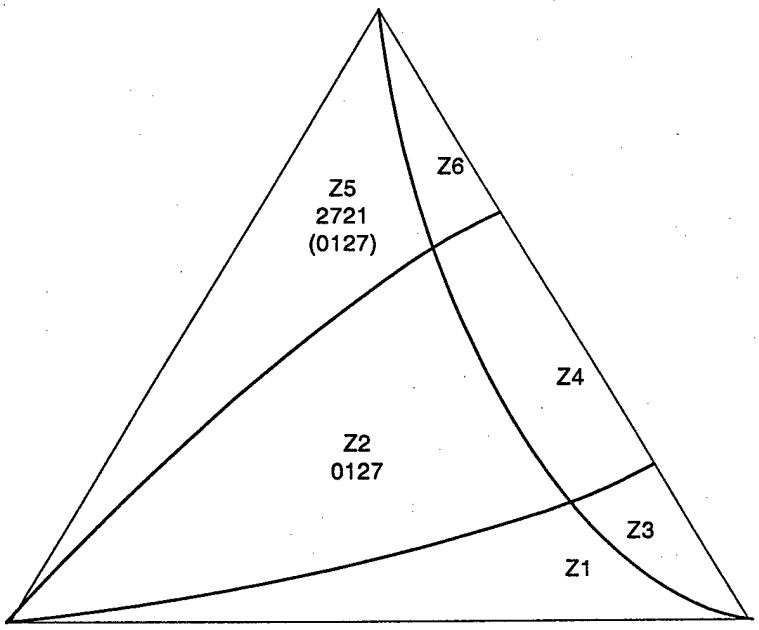

Fig. 53. Hybrid PWM technique using power factor angle and instantaneous current feedback shown in space vector plane (Sector I). Sequences used in each zone are given in Table III

TABLE II – ZONE DEFIINITIONS CORRESPONDING TO PWM TECHNIQUE OF FIG. 53

Zone	Spatial angle, α	First choice sequence	Second choice sequence if first choice results in double switching at current peak
Z1	$\alpha \le \phi - 60°$	1012	N/A
	$\alpha \ge \phi - 60°$	0127	N/A
Z2	All	0127	N/A
Z3	$\alpha \le \phi - 60°$	1012	N/A
	$\alpha \ge \phi - 60°$	7212	0127
Z4	$\alpha \ge \phi + 30°$	0121	N/A
	$\alpha \le \phi + 30°$	7212	0127
Z5	All	2721	0127
Z6	$\alpha \ge \phi + 30°$	0121	N/A
	$\alpha \le \phi + 30°$	7212	2721

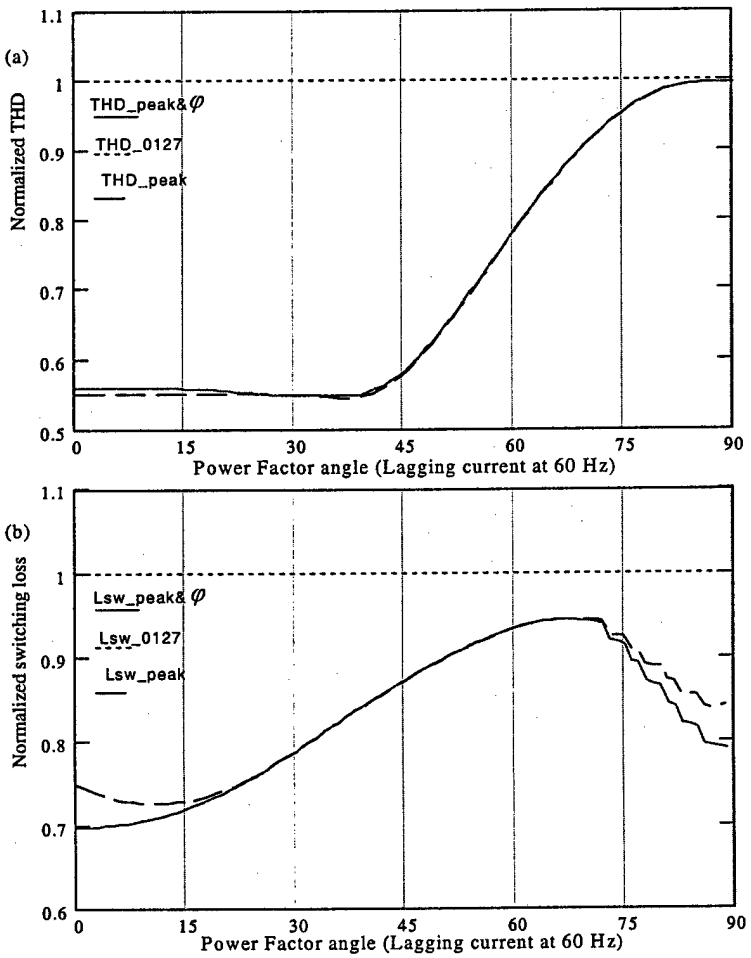

Fig. 54. Simulation results comparing CSVPWM with hybrid PWM techniques shown in Fig. 51 and Fig. 53

The THD and switching loss performance obtained with this PWM technique (Fig. 53), along with that of the conventional SVPWM and current peak detection feedback technique (Fig. 51), are shown in Fig. 54, as a function of power factor angle (corresponding to a fundamental frequency of 60 Hz). It can be seen from the figures that with the power factor angle feedback, the switching loss performance at power factors near 0^0 and beyond 60^0 is improved further without increasing the current THD.

In the experimental setup, the required current feedback for all the three phases is implemented using Hall-effect sensors and on chip Analog/Digital converter of TMS320F243 module from Texas Instruments. The best result in terms of reduction in THD is achieved at maximum modulation index corresponding to a fundamental frequency of 60 Hz. However, the zero state duration under this condition, becomes smaller than the minimum pulse width set by the hardware implementation (for IGBT shoot through protection, and time to run the DSP program). This results in several pulse being dropped and the THD reduction does not correspond to those predicted by simulation. Therefore, the hybrid PWM technique of Fig. 53 is implemented at a fundamental frequency of 50 Hz.

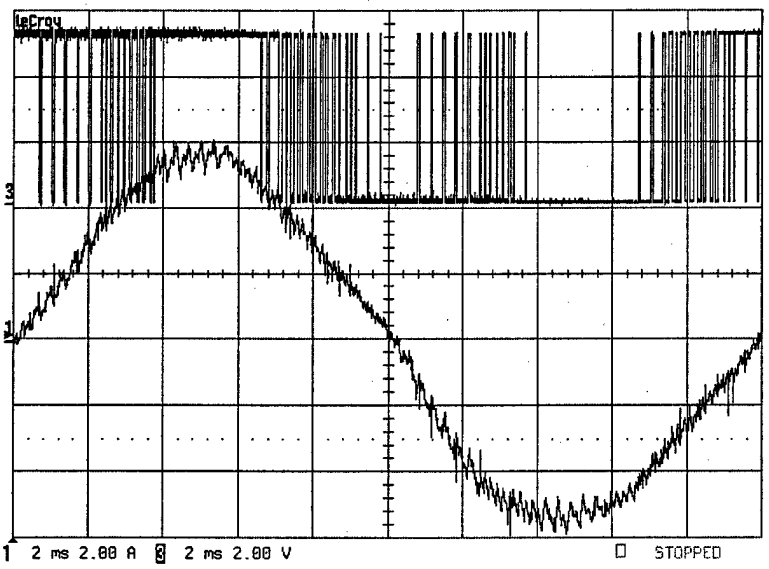

Fig. 55. Experimental PWM and line current waveforms corresponding to hybrid PWM technique shown in Fig. 54, at a power factor angle of 30^0 lagging

Fig. 55 shows the corresponding, experimental PWM and line current waveforms. As seen, the hybrid PWM technique using feedback, results in clamping around the peak of the current resulting in reduced switching losses. The FFT analysis of the phase current waveform shows an 8% reduction in THD (as against 8.8% predicted by analysis) at the power factor angle of 60^0. At the power factor angle of 30^0, the actual reduction in THD is 9.8% (as against 14.2% predicted by analysis). It may be noted that at a fundamental frequency of 60Hz, and a power factor angle of 30^0 lagging, the reduction in THD obtained from analysis is more than 40% compared to conventional, and reduction in switching loss is above 20%.

7. CONCLUSIONS AND FUTURE WORK

The space vector approach to generation of PWM waveform offers several advantages over the traditional triangle comparison methods. However, the conventional sequence *0127* and the existing bus-clamping sequences, *012* and *721* in space vector PWM do not fully exploit these advantages. New sequences, which divide the active vector duration, offer additional degrees of freedom that are not possible in triangle comparison approach. All possible sequences that involve division of active vector duration, and satisfy constraints similar to those of conventional sequences, have been identified in this work. Specifically, four new sequences - *0121, 7212, 1012* and *2721* have been introduced. With the new sequences, it is possible to realize double switching, single switching or zero switching (clamping) of a phase within a sub-cycle, as appropriate, whereas the conventional sequence always results in just single switching per phase per sub-cycle. The number of pulses per sub-cycle in the line-line voltages is also different when the new sequences are used.

In this research project, the concept of stator flux ripple is further developed and applied systematically to compare the effects of the new sequences, as well as conventional sequences, on THD in the line current. For each possible sequence, the zone in the V_{REF}-α plane, where that particular sequence results in minimum THD, is identified. Based on this study, three new hybrid PWM techniques of varying complexity have been designed. Hybrid PWM technique refers to the use of different sequences in different sub-cycles within a sector, unlike the conventional PWM, which applies *0127* throughout Sector I. These hybrid techniques result in as much as 47% reduction in THD in the line current at maximum modulation index, compared to the conventional SVPWM.

The effects of different sequences on the inverter switching loss also have been analyzed in detail. Switching loss in a sub-cycle corresponding to a particular sequence depends on the product of number of switchings of a phase in a sub-cycle and the magnitude of the instantaneous line current of the particular phase in the given sub-cycle. A switching-loss-optimized PWM has been developed by dividing the α–ϕ plane into zones of superior performance for different sequences. This hybrid PWM can reduce the

switching losses by more than 30% compared to the conventional sequence, over a wide range of power factor angles. In general, to minimize the switching losses, the sequence that clamps the phase with the highest current, and double switches the phase whose current is near zero, should be chosen.

Finally, using the results obtained from the independent THD and switching loss studies, new hybrid PWM techniques that simultaneously reduce both THD and inverter switching losses have been developed, specifically for motor drive applications. These techniques achieve a reduction of over 30% in THD and a reduction of over 20% in switching losses ***simultaneously***, while operating at nominal fundamental frequency of 60 Hz and power factor angles close to 30^0 lagging. Hybrid PWM techniques that utilize feedback of instantaneous line currents and power factor angle have also been studied. However, the improvement in performance over hybrid PWM techniques with no feedback, especially in the context of motor drive applications where the range of variation in power factor is limited, is not very significant and does not justify the added complexity. However, if the current feedback is already available, it may be utilized to realize small improvement in switching loss performance.

All the proposed PWM techniques (corresponding to minimum THD, minimum switching loss and simultaneous reduction), as well as the conventional space vector PWM for comparison, have been implemented and validated on an experimental prototype comprising of a 2kW IGBT-based VSI fed induction motor drive controlled by a DSP - TMS320F243. THD reduction of 38% in the THD-optimized PWM and switching loss reduction of 30% in the switching-loss-optimized PWM, over the conventional space vector PWM have been demonstrated experimentally. The clock frequency of 20 MHz for the DSP used has been a limiting factor, since pulses with width less than a certain threshold need to be dropped leading to increased THD. With faster clock frequencies (or lower switching frequency for high power drives), the experimental results are expected to be even closer to the analytical results than what has been demonstrated here.

7.1 Suggestions for Future Work

Possible future work in this area that show promise of further improvement in the performance of induction motor drives are listed below.

A: Analysis of the effect of new sequences on the input current drawn by the converter from the DC source. The DC link current has an appreciable impact on the rating and reliability of the DC link capacitor. Hence, PWM techniques that minimize ripple in the input current can enhance the reliability of the input capacitor, and hence, the overall drive system.

B: In the present study, the active state duration (as well as zero state duration) is divided equally into two intervals, to form new sequences. Unequal division of active vector duration can lead to further improvement in steady state performance.

C: The present study has focused solely on three-phase, two-level converters, which have only eight states. Multi-level PWM converter has been a subject of vigorous research recently. With a total of n^3 possible states, the multi-level PWM can reduce the THD significantly, though at the expense of increased control complexity. The concept of division of active state duration can be investigated for multi-level converters to achieve improved performance in terms of THD, switching loss and input current ripple.

REFERENCES

[1] J. Holtz, "Pulsewidth modulation – a survey," *IEEE Transactions on Industrial Electronics*, vol. 39, No. 5, December 1992, pp. 410–420.

[2] J. Holtz, "Pulsewidth modulation for electronic power conversion," *Proceedings of the IEEE*, vol. 82, No. 8, August 1994, pp. 1194–1214.

[3] H. Stemmler, "High-power industrial drives," *Proceedings of the IEEE*, vol. 82, No. 8, August 1994, pp. 1266–1286.

[4] A. M. Hava, R. J. Kerkman, and T. A. Lipo, "Simple analytical and graphical methods for carrier-based PWM-VSI drives," *IEEE Transactions on Power Electronics*, vol. 14, No. 1, January 1999, pp. 49-61.

[5] J.W.Kolar, H.Ertl and F.C.Zach, "Influence of the modulation method on conduction and switching losses of a PWM converter system", IEEE Trans. IA, Vol. IA-27(6), 1991, pp.1063-1075.

[6] R. D. Adams, and R.S Fox, "Several modulation techniques for a Pulsewidth modulated inverter," *IEEE Transactions on Industrial Applications,* vol. 8, No. 5, 1972, pp. 636-643.

[7] P. G. Handley, and J. T. Boys, "Practical real-time PWM modulators – An assessment," *Proceedings of the IEE,* vol. 139, No. 2, 1992, pp. 96-102.

[8] J.W.Kolar, H.Ertl and F.C.Zach, "Minimising the current harmonics RMS value of three-phase PWM converter system by optimal and suboptimal transition between continuous and discontinuous modulation", 22nd IEEE Annual Power Electronics Specialists' Conf., PESC '91, Cambridge, MA, USA, June 1991, pp. 372-381.

[9] A.M.Hava, T.A.Lipo and R.J.Kerkman, "Carrier-based PWM-VSI overmodulation strategies : analysis, comparison and design", IEEE Trans. PE, Vol. PE-13(4), 1998, pp. 674-689.

[10] V. Blasko, "Analysis of a hybrid PWM based on modified space-vector and triangle-comparison methods," *IEEE Transactions on Industrial Applications,* vol. 33, No. 3, May/June 1997, pp. 756-764.

[11] K. Zhou, and D. Wang, "Relationship between space-vector modulation and three-phase carrier-based PWM: A comprehensive analysis," *IEEE Transactions on Industrial Electronics*, vol. 49, No. 1, February 2002, pp. 186–196.

[12] D.G.Holmes, "The significance of zero space vector placement for carrier-based PWM schemes", IEEE Trans. IA, Vol. IA-32(5), 1996, pp. 1122-1129.

[13] H.W. van der Broeck, "Analysis of the harmonics in voltage fed inverter drives caused by PWM schemes with discontinuous switching operation," *4th European Conference on Power Electronics and Applications, EPE'91*, pp. 261-266, 1991.

[14] S. Fukuda and K. Suzuki, "Harmonic evaluation of two-level carrier-based PWM methods," *7th European Conference on Power Electronics and Applications, EPE'97*, pp. 231-336, 1997

[15] R.M.Green and J.T.Boys, "PWM sequence selection and optimisation : A novel approach", IEEE Trans. IA, Vol. IA-18(2), 1982, pp. 146-151.

[16] M.A.Boost and P.D.Ziogas, "State-of-the-art carrier PWM techniques : a critical evaluation", IEEE Trans. IA, Vol. IA-24(2), 1988, pp. 271-280.

[17] G. Narayanan, and V. T. Ranganathan, "Synchronised PWM strategies based on space vector approach: I – Principles of waveform generation," *IEE Proceedings on Electric Power Applications*, vol. 146, No. 3, May 1999, pp. 267-275.

[18] G. Narayanan, and V. T. Ranganathan, "Two novel synchronized bus-clamping PWM strategies based on space vector approach for high power drives," *IEEE Transactions on Power Electronics*, vol. 17, No. 5, September 2002, pp. 84-93

[19] D.J.Tooth, S.J.Finney and B.W.Williams, "Fourier theory of jumps applied to converter harmonic analysis," IEEE Trans. Aerospace and Electronic Systems, vol. 37(1), pp. 109-122, Jan 2001.

[20] J.T.Boys and P.G.Handley, "Harmonic analysis of space vector modulated PWM waveforms," IEE Proc. B, vol. 137(4), pp. 197-204, July 1990.

APPENDIX A: LIST OF PUBLICATIONS FROM THIS WORK

1. D. Zhao, G. Narayanan, R. Ayyanar, " Switching loss characteristics of sequences involving active state division in space vector based PWM," *Proc. IEEE Applied Power Electronics Conference (APEC'04),* Feb. 2004.

2. H. Krishnamurthy, G. Narayanan, R. Ayyanar, V.T. Ranganathan, "Design of space vector based hybrid PWM techniques for reduced current ripple," *Proc. IEEE Applied Power Electronics Conf. (APEC'03)*, vol. 1, 2003, pp. 583-588.

3. Harish K. Krishnamurthy, "Space vector methods for ac drives to achieve high efficiency and superior waveform quality", M.S. thesis, Arizona State University, Apr. 2003.

4. G. Narayanan, H. Krishnamurthy, D. Zhao, R. Ayyanar, "Advanced Bus-Clamping PWM Techniques Based on Space Vector Approach," submitted to IEE Proceedings on Electric Power Applications.